



HAL
open science

Single-cell transcriptomic landscape reveals tumor specific innate lymphoid cells associated with colorectal cancer progression

Jingjing Qi, Adeline Crinier, Bertrand Escalière, Youqiong Ye, Zhengting Wang, Tianyu Zhang, Luciana Batista, Hongzhi Liu, Liwen Hong, Ningbo Wu, et al.

► To cite this version:

Jingjing Qi, Adeline Crinier, Bertrand Escalière, Youqiong Ye, Zhengting Wang, et al.. Single-cell transcriptomic landscape reveals tumor specific innate lymphoid cells associated with colorectal cancer progression. *Cell Reports Medicine*, 2021, 2 (8), pp.100353. 10.1016/j.xcrm.2021.100353 . hal-03374574

HAL Id: hal-03374574

<https://amu.hal.science/hal-03374574>

Submitted on 22 Aug 2023

HAL is a multi-disciplinary open access archive for the deposit and dissemination of scientific research documents, whether they are published or not. The documents may come from teaching and research institutions in France or abroad, or from public or private research centers.

L'archive ouverte pluridisciplinaire **HAL**, est destinée au dépôt et à la diffusion de documents scientifiques de niveau recherche, publiés ou non, émanant des établissements d'enseignement et de recherche français ou étrangers, des laboratoires publics ou privés.



Distributed under a Creative Commons Attribution - NonCommercial 4.0 International License

1 **Single cell transcriptomic landscape reveals tumor specific innate lymphoid cells associated**
2 **with colorectal cancer progression**

3 Jingjing Qi^{1,2#}, Adeline Crinier^{3#}, Bertrand Escalière³, Youqiong Ye^{1,2}, Zhengting Wang⁴, Tianyu
4 Zhang⁴, Luciana Batista⁵, Hongzhi Liu^{1,2}, Liwen Hong⁴, Ningbo Wu¹, Mingnan Zhang¹, Lei Chen¹,
5 Yingbin Liu⁷, Lei Shen^{1*}, Emilie Narni-Mancinelli^{3*}, Eric Vivier^{3,5,6*}, & Bing Su^{1,2,8*}

6

7 ¹Shanghai Institute of Immunology, Department of Immunology and Microbiology, and the
8 Ministry of Education Key Laboratory of Cell Death and Differentiation, Shanghai Jiao Tong
9 University School of Medicine, Shanghai, 200025, China

10 ²Shanghai Jiao Tong University School of Medicine-Yale Institute for Immune Metabolism,
11 Shanghai Jiao Tong University School of Medicine, Shanghai, 200025, China

12 ³Aix Marseille Univ, CNRS, INSERM, Centre d'Immunologie de Marseille-Luminy, Marseille,
13 13009, France

14 ⁴Department of Gastroenterology, Ruijin Hospital, Shanghai Jiao Tong University School of
15 Medicine, Shanghai, 200025, China

16 ⁵Innate Pharma Research Laboratories, Innate Pharma, Marseille, 13009, France

17 ⁶Immunology, Marseille Immunopole, Hôpital de la Timone, Assistance Publique des Hôpitaux de
18 Marseille, 13005, France

19 ⁷Department of General Surgery, Xinhua Hospital Affiliated to Shanghai Jiao Tong University
20 School of Medicine, Shanghai 200092, China

21 ⁸Lead Contact

22 # These authors contributed equally

23 *Correspondence: lshen@shsmu.edu.cn; narni@ciml.univ-mrs.fr; vivier@ciml.univ-mrs.fr;

24 bingsu@sjtu.edu.cn

25 **Summary**

26 Innate lymphoid cells (ILCs) are tissue-resident lymphocytes **differing** from conventional T
27 lymphocytes in having no antigen-specific receptors. ILCs include natural killer (NK) cells,
28 helper-like ILC1s, ILC2s, ILC3s and lymphoid tissue-inducer (LTi) cells. Tumor ILCs are
29 frequently found in various cancers, but their roles in cancer immunity and immunotherapy remain
30 **largely unclear**. We report here the single-cell characterization of blood and gut helper-like ILC
31 subsets in healthy conditions and in colorectal cancer (CRC). The healthy gut contains ILC1s,
32 ILC3s, and ILC3/NKs, but no ILC2s. Additional tumor-specific ILC1-like and ILC2 subsets were
33 identified in CRC patients. Signaling lymphocytic activation molecule family member 1
34 (SLAMF1) was found to be selectively expressed on tumor-specific ILCs and higher levels of
35 SLAMF1⁺ ILCs were observed in the blood of CRC patients. The SLAMF1-high group of **CRC**
36 patients had a significantly higher survival rate than the SLAMF1-low group, suggesting that
37 SLAMF1 is an anti-tumor biomarker in CRC.

38 **Introduction**

39 T cell-based immunotherapy has been very successful clinically for the treatment of malignant
40 tumors, but only in a small proportion of patients ¹⁻⁶. Treatments targeting other immune
41 components are required, to increase the proportion of patients benefiting from immunotherapy.
42 Innate lymphoid cells (ILCs) are tissue-resident innate antigen-independent lymphocytes that
43 regulate immunity to pathogens and commensal organisms for tissue homeostasis ^{7,8}. ILCs form a
44 heterogeneous population of cells that are currently classified into five major groups, natural killer
45 (NK) cells, helper-like ILC1s, ILC2s, ILC3s, and lymphoid tissue-inducer (LTi) cells on the basis
46 of their cytokine production and transcription factor expression profiles ⁸. ILCs are involved in
47 immune functions, including pathogen responses, inflammation, tissue development, remodeling,
48 repair and homeostasis.

49 Given the large amounts and nature of the cytokines they produce, ILC subsets are likely to be
50 involved in cancer immunity, but may also contribute to tumor-associated inflammation. NK cells
51 are known to play a role in cancer, through their tumor-suppressive properties, and are efficient at
52 controlling metastasis ⁹. The role of **helper-like** ILCs in the context of tumorigenesis and cancer
53 immunity is less clear and appears to depend on the tumor microenvironment. ILC1s produce
54 large amounts of proinflammatory cytokines, such as IFN- γ and TNF- α , which favor
55 tumorigenesis ¹⁰. However, IFN- γ can also limit tumor growth in certain tumor
56 microenvironments ^{11, 12}. ILC2s have been shown to be mostly detrimental in various tumor
57 settings. Indeed, large numbers of ILC2s are present in the peripheral blood of patients with
58 gastric cancer ¹³ and acute promyelocytic leukemia ¹⁴. ILC2-derived IL-13 stimulates the
59 immunosuppressive activity of myeloid-derived suppressor cells in acute promyelocytic leukemia
60 ¹⁴, and in human bladder cancer and murine prostate tumors ¹⁵. However, ILC2-derived IL-5 may

61 help to suppress primary and metastatic lung tumors in mouse models ^{16, 17}. ILC2 could also
62 secrete CXCR2 ligands to reinforce tumor cell-specific apoptosis in solid tumor mouse model ¹⁸,
63 and ILC2s activate tissue-specific tumor immunity in pancreatic cancer ¹⁹. ILC3s also have tumor
64 suppressor properties, in the B16 melanoma mouse model ^{20, 21} and in non-small cell lung cancer
65 (NSCLC) patients ²², for example. By contrast, ILC3-derived IL-17 and IL-22 may contribute to
66 gut cancer development ^{23, 24}. There is, therefore, a clear need to investigate the presence and role
67 of helper-like ILC subsets in various cancer indications.

68 Colorectal cancer (CRC) is the third most prevalent cancer in both women and men, and the
69 second most frequent cause of cancer-related deaths worldwide ²⁵, despite remarkable
70 improvements in therapeutic strategies. Dysregulated ILC responses have been linked to the
71 development of intestinal cancers. ILC2s are present at low levels in many pathological
72 conditions in humans ^{26, 27}. By contrast, CRC patients have large numbers of ILC1s in the
73 intestines ²⁶⁻²⁹, and abnormally low levels of ILC3s ^{28, 29}, which normally densely populate the
74 colon at steady state ²⁷⁻²⁹. Indeed, decreases in the ILC3/ILC1 ratio have been associated with the
75 severity of CRC ²⁹. The baseline helper-like ILC landscape, in terms of the composition,
76 diversity, and functional status of these cells in the human gut, remains incompletely explored
77 under tumor conditions.

78 We used unsupervised hierarchical clustering to investigate helper-like ILC heterogeneity at
79 steady state and during CRC, in the blood, normal mucosa and gut tumors. The healthy gut is
80 composed of ILC1s, ILC3s, and ILC3/NKs, but no ILC2s. Helper-like ILCs from CRC patients
81 were found to contain two additional subsets: a CRC tissue-specific ILC1-like subset (ctILC1-
82 like) and an ILC2 (ctILC2) subset. SLAMF1 (signaling lymphocytic activation molecule family
83 member 1, CD150) was found to be selectively expressed on ctILCs, and higher frequencies of

84 SLAMF1-expressing helper-like ILCs were found in the blood of CRC patients. The group of
85 patients with SLAMF1-high colon and rectal cancers had a significantly higher survival rate than
86 the SLAMF1-low patients, suggesting that SLAMF1 is an anti-tumor biomarker in CRC.

87 **Results**

88 **Healthy gut contains ILC1s, ILC3s, and ILC/NKs, but no ILC2s**

89 We dissected the role of helper-like ILCs in CRC by studying paired CRC tissue and adjacent
90 mucosal tissue (used as a control) samples, and comparing blood from patients with blood from
91 age-matched healthy donors (Table S1 and Figure S1A). Lineage negative (Lin^-) ($TCR\gamma\delta^-$ TCR
92 $\alpha\beta^-$ $CD3^-$ $CD19^-$ $CD14^-$ $CD16^-$ $CD94^-$ $CD123^-$ $CD34^-$ $CD303^-$ $Fc\epsilon RI^-$) $CD127^+$ helper-like ILCs
93 were more abundant in both normal mucosa and CRC tissue than in blood, consistent with the
94 known tissue residence properties of ILCs³⁰ (Figure S1B-C). The percentage of helper-like ILCs
95 was lower in CRC tissues than in normal mucosa, but similar in normal and CRC blood samples
96 (Figure S1B-C).

97 We performed scRNAseq on ~58,000 total purified helper-like ILCs from blood samples from
98 CRC patients, healthy blood, normal mucosa and CRC tissue samples (Figure S1D-E). The
99 heterogeneity of helper-like ILCs in normal mucosa was assessed with a total of 16,145 Lin^-
100 $CD127^+$ cells from colon tissues adjacent to the colon tumor in CRC patients (Figure S1E). The
101 projection of cells onto two dimensions in a uniform manifold approximation and projection
102 (UMAP) analysis revealed segregation into six distinct clusters: normal mucosa cluster (nmC)0 to
103 nmC5 (Figure 1A). Two clusters, nmC4 and nmC5, contained cells from all donors, suggesting
104 that there was no donor-specific transcriptomic profile for these two helper-like ILC populations
105 (Figure 1B-C). By contrast, most of the cells from nmC0 to nmC3 were single donor-specific
106 (Figure 1B-C).

107 Using hierarchical clustering (Figure 1C) and gene signature heatmaps (Figure 1D and Table S2),
108 principal component analysis (PCA) (Figure 1E-F), top 10 expressed gene analysis (Figure 1G),
109 and module score analysis (Figure 1H), we then compared the gene signatures of nmC0 to nmC5

110 with previously described transcriptomic signatures of human helper-like ILC subsets³¹. nmC0 to
111 nmC3 had a common transcriptomic signature characteristic of ILC3s, with *REL*, encoding a
112 proto-oncogene member (c-Rel) of the NF-κB family³² and NF-κB signaling *via* the *IL22*
113 promoter site in ILC3s³³, as a driver gene (Figure 1F), and *KIT*, *CXCL8*, *IL411* and *IL1R1* in the
114 top 10 expressed genes (Figure 1G). nmC4 was characterized by *NKG7*, encoding a cytolytic
115 granule membrane protein³⁴, and *KLRD1*, encoding CD94, expressed in T and NK cells, as driver
116 genes, with *GNLY*, *GZMK*, *XCL2*, and *CCL4*, among the top expressed genes and with a whole
117 signature common to NK cells and ILC3s from tonsils (Figure 1F-G). nmC4 was, thus, identified
118 as an ILC3/NK subset. nmC5 resembled ILC1s, with higher levels of expression of T-cell markers
119 (*CD3D*, *CD3G*, and *CD3E*), as previously described^{31,35,36}, specific transcription factors (*IKZF3*,
120 *BCL11B*, *PRDM1*, and *ID3*), and NK/ILC1 cell functional cytokines (*GZMM*, *IFNG*, *IL32*, *CCL4*,
121 and *CCL5*) (Figure 1F-H). nmC0-3 were enriched in response to lipid, glucocorticoid, and
122 corticosteroid while nmC5 was involved in T cell activation and differentiation (Figure S2A). The
123 assignments of each cluster were supported by the selective expression of known helper-like ILC
124 markers, such as *IL7R*, *GATA3*, *NCR3*, *EOMES*, *TBX21*, *KIT*, *RORC*, *NCR1*, *NCR2* and *KLRF1*
125 (Figure S2B). We found differences between nmC5 and previously reported healthy gut ILC1s³⁷,
126 probably because the gating strategies used here did not exclude CD5⁺ cells (Figure S2C-D). Thus,
127 the normal gut mucosa defined by scRNAseq profiling of Lin⁻CD127⁺ contains ILC1s, ILC3s, and
128 ILCs/NKs but no ILC2s, consistent with the lack of *PTGDR2* gene expression (Figure S2B).

129

130 **Tumor ILC1-like and ILC2 subsets are present in CRC patients**

131 We then investigated the composition and diversity of 15,101 ILCs from the tumors of CRC
132 patients. UMAP analysis identified four distinct clusters in CRC tissue (ctC short for CRC tissue

133 cluster): ctC0 to ctC3 (Figure 2A). Contrary to what was observed for normal mucosa, no
134 overwhelming donor-dependent effect was observed, each cluster being present in all samples
135 (Figure 2B-C). Based on the strategy applied to normal mucosa clusters (Figure 1), ctC0 was
136 assigned to ILC3s, consistent with its overexpression of *KIT*, *CXCL8*, *NFIL3*, and *IL411*, like
137 nmC0-3 (Figure 2C-H and Table S2). ctC1 resembled ILC1s and, like nmC5, displayed
138 differential expression of genes encoding T-cell molecules (*CD3D*, *CD3G*), secreted effectors
139 (*CCL4*, *IFNG*), and ILC-related transcription factors (*IKZF3*, *PRDM1* and *BCL11B*). The other
140 two subsets present, ctC2 and ctC3, were absent from normal mucosa. ctC2 cells corresponded to
141 an additional ILC1 subset, hereafter called the ctILC1-like subset (CRC tissue-specific ILC1-like
142 subset), characterized by an enrichment in the expression of genes encoding inhibitory and
143 costimulatory markers (*TIGIT*, *CTLA4*, and *TNFRSF4*). ctC3 cells, identified as ILC2s and
144 hereafter referred to as ctILC2, had high levels of expression for genes encoding transcription
145 factors required for ILC2 development (*GATA3*, *RORA*, and *ZBTB16*) and ILC2-responsive
146 cytokine receptor genes (*IL1RL1* and *IL17RB*) (Figure 2C-H and Table S2). ctC1 was enriched in
147 cytolysis, granulocyte chemotaxis, granzyme-mediated apoptotic signaling pathway, whereas ctC2
148 and ctC3 were respectively enriched in T cell anergy and interleukin-5 production and interleukin-
149 13 secretion (Figure S2E). Subset assignments were supported by the selective expression of
150 known ILC markers, such as *IL7R*, *GATA3*, *NCR3*, *EOMES*, *TBX21*, *KIT*, *RORC*, *NCR1*, *NCR2*
151 and *KLRF1* (Figure S2F). In particular, *PTGDR2* and higher levels of *GATA3* expression were
152 found in the ILC2s. *SLAMF1* (signaling lymphocytic activation molecule family member 1 or
153 CD150), which encodes a soluble and membrane protein involved in the activation of T cells, B
154 cells, and NK cells³⁸, was upregulated both in ctILC1-like and ctILC2 in tumors (Figure 2G).
155 Thus, like nmILCs, ctILCs formed heterogeneous populations encompassing four different subsets:

156 ctC0 (resembling ILC3s), ctC1 (resembling ILC1s), ctC2 (named as ILC1-like), and ctC3
157 (resembling ILC2s).

158 Tumor tissue ILC3s seemed to be less heterogeneous than those in the normal mucosa. We
159 therefore focused on nmC0-3, nmC4 and ctC0, comparing ILC3 heterogeneity between normal
160 mucosa helper-like ILCs and gut ctILCs, with the same analysis pipeline as described above after
161 applying a correction that removed the donor batch effect allowing the analysis of ILC3
162 heterogeneity (Figure S3, Table S2). Four different populations were found in ILC3s from both
163 types of tissue (Figure S3 A-I), including a potentially immature *SELL*-expressing population, and
164 a population enriched in HLA-encoding transcripts also present in human tonsils (Figure S3E and
165 J). Each subset of normal mucosa ILC3 had a counterpart in tumor tissue (Figure S3K). Given the
166 overlap in ILC3s heterogeneity between normal mucosa and gut ctILCs, we can conclude that
167 CRC did not affect the subset heterogeneity of ILC3s. Thus, gut ctILCs differed from nmILCs in
168 the appearance of a ctILC2 subset and a second ctILC1-like subset.

169

170 **Blood helper-like ILC heterogeneity is stable in CRC**

171 We searched for potential biomarkers of the disease, by investigating differences in blood helper-
172 like ILCs between healthy individuals and CRC patients. A UMAP analysis of 19,603 helper-
173 like ILCs from healthy donors revealed three distinct clusters, hereafter referred to as nbC0,
174 nbC1, and nbC2 (Figure S4A-C and Table S2). nbC0 was considered to correspond to ILC1s,
175 based on the upregulation of *CD3D*, *CD3E*, *CD3G*, the NK/ILC1 cell effector proteins (*CCL5*,
176 *GZMK*, *GZMM*, and *GZMA*), and helper-like ILC transcription factors (*BCL11B*, *PRDM1*, and
177 *IKZF3*) (Figure S4D-H). nbC1 was identified as ILC3s, and was characterized by ILC3
178 transcription factors (*MAFF*, *RUNX3*) and costimulation markers (*TNFRSF4*, *TNFRSF18*). nbC2

179 displayed an upregulation of genes from the ILC2 signature (*GATA3*, *RORA*), and genes
180 encoding regulatory receptors (*KLRB1*, *KLRG1*) (Figure S4D-H). These assignments were
181 supported by the selective expression of known helper-like ILC markers, such as *IL7R*, *GATA3*,
182 *NCR3*, *EOMES*, *TBX21*, *PTGDR2*, *KIT*, *RORC*, *NCRI*, and *KLRF1* (Figure S4I).

183 A UMAP plot of 6,899 blood helper-like ILCs from CRC donors also identified three subsets,
184 hereafter referred to as cbC0, cbC1 and cbC2 (Figure S5A-C and Table S2). Driver genes, top
185 ten genes and module score signatures highlighted the similarity of cbILCs to nbILCs (Figure
186 S5D-H). cbC0, like nbC1, had an ILC3 profile with enrichment for *MAFF*, *RUNX3*, *TNFRSF18*.
187 cbC1 were identified as ILC2s, with high levels of *RORA*, *KLRB1*, *KLRG1*, and *PTGDR2*
188 expression, like nbC2. Of note, similar to ctILC2, cbC1 exhibited high levels of *SLAMF1*. cbC2,
189 like nbC0, displayed an enrichment in the genes of the ILC1 signature: *CD3D*, *CD3G*, *CD3E*,
190 *CCL5*, *GZMK*, *GZMM*, *GZMA*, *BCL11B*, *PRDM1*, and *IKZF3* (Figure S5D-I). These
191 assignments were also supported by the selective expression of *IL7R*, *GATA3*, *NCR3*, *EOMES*,
192 *TBX21*, *PTGDR2*, *KIT*, *RORC*, *NCRI*, and *KLRF1* (Figure S5I). However, despite the similarity
193 of cbILC subsets to nbILC subsets, velocity analysis predicted a possible conversion of ILC1s
194 into ILC3s only in the context of CRC, in tumor blood (Figure S5J and data not shown). In
195 summary, the blood helper-like ILCs of both healthy donors and CRC patients formed
196 heterogeneous populations containing ILC1, ILC2 and ILC3 subsets.

197

198 **Identification of a population of CRC tissue-specific ILC1s**

199 Tumor tissue helper-like ILCs contained two additional populations not present in the helper-like
200 ILCs of the normal mucosa, with transcriptomic signatures resembling those of ILC2s and ILC1s
201 (Figure 1 and Figure 2). We investigated the relatedness of these two tumor tissue-specific

202 clusters and the helper-like ILC subsets from healthy blood and blood from CRC patients, by
203 grouping the 41,603 helper-like ILCs into a single global analysis. This analysis revealed organ-
204 specific imprinting in helper-like ILCs, with an overlap between the two types of blood samples,
205 and ctILCs clustering separately (Figure 3A and Table S2). There was a high degree of similarity
206 between nbILCs and cbILCs in gene signature, it was remarkably different from that of ctILCs
207 (Figure 3B-C). We further investigated the relationship between defined ILC subsets from CRC
208 tissue, normal blood and CRC blood samples. The ctILC1-like subset appeared to segregate
209 away from the other clusters, including TILC1 in particular, despite having a core ILC1-
210 transcriptomic signature in common with this subset (Figure 3D). Likewise, another TILC-
211 specific subset, ctILC2, clustered away from the other ctILCs and the ILC2 in the blood. In the
212 blood, each nbILC clustered with the corresponding cbILC subset (Figure 3D). We investigated
213 whether the tumor-specific helper-like ILCs shared more genes to their normal blood or CRC
214 blood counterparts, by creating Venn diagrams comparing their whole transcriptomic signatures
215 (Figure 3E-F). The ctILC1-like subset shared more genes with cbILC1 (57 genes in common)
216 than with nbILC1 (34 genes in common) (Figure 3E), suggesting a tumor imprinting, whereas
217 ctILC2 shared comparable numbers of genes with cbILC2 and nbILC2, with which this subset
218 had 39 and 34 genes, respectively, in common (Figure 3F).

219

220 **Helper-like ILC signature is modified in CRC tumor**

221 We searched for tumor-specific tissue features of ILCs, by clustering the 31,246 helper-like ILC
222 cells from normal mucosa and tumor tissues. These two tissues had some helper-like ILC
223 populations in common, but UMAP highlighted a shift between the two tissues, suggesting
224 differences at the transcriptomic level (Figure 4A). Unsupervised hierarchical clustering also

225 showed the tissue-of-origin signature to be stronger than the helper-like ILC subset identity
226 signature (Figure 4B-C, Table S2). The clustering of nbILCs and cbILCs revealed a similar pattern
227 of separation for the 26,502 helper-like ILCs in the UMAP analysis (Figure 4D), and in
228 unsupervised hierarchical clustering, which segregated blood samples according to health status,
229 revealing differences in transcription between the two subsets (Figure 4E-F). One gene was found
230 to be upregulated in normal blood and mucosa (*AQP3*). Four genes were identified as upregulated
231 in both CRC blood and gut ctILCs relative to their healthy counterparts (*SLAMF1*, *HPGD*, *TLE4*,
232 and *PRDMI*) (Figure 4G). Feature plots of these five genes of interest confirmed the specific
233 upregulation of *SLAMF1*, *HPGD*, *TLE4*, and *PRDMI* in gut ctILCs, and the downregulation of
234 *AQP3* (Figure 4H-I). *SLAMF1* was the principal surface protein gene upregulated in tumors. This
235 gene was expressed in ctILC2, ctILC1-like subsets and cbILC2 (Figure 2G, 4H and Figure S5),
236 but only weakly in their healthy counterparts (Figure 4H), suggesting that *SLAMF1* expression at
237 the helper-like ILC cell surface can differentiate healthy individuals from CRC patients.

238

239 **SLAMF1 is a biomarker of CRC**

240 We confirmed, by flow cytometry, the expansion of the ILC1 subset accompanied by reduction
241 of the ILC3 subset in tumor tissues from CRC patients relative to adjacent normal mucosa
242 (Figure 5A-B). Consistent with the scRNAseq analysis revealing higher levels of *TIGIT* in an
243 ILC1-like subset and the presence of ctILC2s (Figure 2G), we observed by flow cytometry a
244 population of *TIGIT*⁺ ctILC1-like cells and ctILC2 in tumors, but not in normal tissue (Figure
245 5A-B). Higher levels of expression of the ILC2-activating cytokine *IL33* in tumors were
246 correlated with longer survival in CRC patients from The Cancer Genome Atlas (TCGA) dataset,
247 suggesting that ctILC2 might be indicative of a good prognosis in CRC patients (Figure 5C). In

248 contrast to the findings for gut helper-like ILCs, the frequency of each helper-like ILC subset
249 among total helper-like ILCs in blood was similar in CRC patients and healthy donors (Figure
250 5D). Larger numbers of ILCs expressing SLAMF1 at their surface was found in tumors than in
251 the adjacent tissues, from which SLAMF1 was almost absent (Figure 5E-F). By contrast,
252 SLAMF1 was expressed by blood ILCs from healthy donors, but high frequencies of SLAMF1-
253 expressing helper-like ILCs were also found in the blood of CRC patients (Figure 5G).
254 Signatures of *SLAMF1*⁺ and *SLAMF1*⁻ ILCs from CRC tissue were then compared. While *RORA*
255 and *IL32* expression were relatively high in *SLAMF1*⁺ ILCs, *XCL2* and *XCL1* expression were
256 enriched in *SLAMF1*⁻ ILCs (Figure 5H). IL-32 was reported to be anti-tumor in several cancer
257 types, including cervical, colon, prostate, liver and pancreatic cancer, as well as melanoma and
258 chronic myeloid leukemia ³⁹, suggesting that *SLAMF1*⁺ ILCs might exhibit an *IL-32* dependent
259 anti-tumor effect. We then investigated the potential role of SLAMF1 in CRC disease
260 development and progression further, by studying the clinical outcome of cancer patients from
261 the TCGA database. Survival was much higher in patients with *SLAMF1*-high colon and rectal
262 cancer than in those with *SLAMF1*-low tumors (Figure 5I-J), strongly suggesting that SLAMF1
263 is an anti-tumor biomarker in CRC.

264 **Discussion**

265 Over the last decade, helper-like ILCs have emerged as key elements in protection against
266 pathogens, tissue remodeling and homeostasis ⁸. The contribution of helper-like ILCs to cancer
267 remains poorly understood, as they may promote tumor-associated inflammation or, conversely,
268 may display anti-tumor properties, depending on the tumor microenvironment.

269 We investigated the heterogeneity of helper-like ILCs in the human gut and blood by building a
270 single cell transcriptomic landscape of Lin⁻CD127⁺ cells at steady state and in CRC patients.
271 This unbiased helper-like ILC characterization differed from the analysis of gut ILC
272 transcriptomes provided by another recent study, in which these cells were subjected to sorting
273 by flow cytometry on the basis of the CD103, CD300LF and CD196 cell surface markers before
274 transcriptomic profiling ⁴⁰. We show here by single-cell RNA sequencing that the healthy gut
275 contains ILC1s, ILC3s, a population of ILC3/NKs, but no ILC2s. Indeed, only few ILC2s can be
276 detected by flow cytometry as Lin⁻CRTH2⁺ in our analysis and in ⁴¹. In a recent study ³⁷, only 2
277 donors out of 18 exhibited reliable ILC2 population in colon lamina propria (2.7% and 3.9% of
278 Lin⁻CRTH2⁺), but the vast majority (16 donors) did not possess a solid ILC2 subset (0 to 0.6%
279 of Lin⁻CRTH2⁺). Thus, purification of these cells for RNA sequencing was not successfully
280 achieved ³⁷. Importantly, even if few ILC2s may be present in the intestine of some donors, these
281 cells did not give rise to a robust cluster detectable by scRNA sequencing taking into account the
282 minimal percentage of cells needed to exclude a possible doublet contamination. Indeed, and by
283 contrast to what has been reported for mice, ILC2s are almost entirely absent from healthy
284 human tissues, with the exception of the lungs, adipose tissue and the blood connective tissue ⁴¹.
285 In our study, we detected tumor infiltrating ctILC2 in CRC patients. ctILC2 were also observed
286 in breast ⁴², gastric ⁴², and pancreatic ¹⁹ tumors and in urine from bladder cancer patients ¹⁵.

287 Several data support a model in which ILC2s infiltrate tumors via an IL-33-dependent pathway ¹⁵,
288 ^{16, 19} and mediate tumor immune surveillance by promoting cytolytic CD8⁺ T-cell responses. IL-
289 33 expression showed different survival prognosis in different cancer types, with better
290 prognosis in melanoma patients but not in lung squamous cell carcinoma and pancreatic
291 adenocarcinoma ⁴³. IL-33 is overexpressed in colorectal tumors ⁴⁴ and high levels of IL-33 are
292 frequently observed in low-grade adenocarcinomas and early colorectal tumors ⁴⁵. Survival rate
293 is higher in the IL-33-high group of colon cancer patients than in IL-33-low patients, suggesting
294 that ctILC2 might be indicative of a good prognosis in CRC. However, PD-1 expression on
295 ctILC2 from late stage of CRC may be of bad prognosis ⁴⁶. There is, therefore, a clear need to
296 investigate further the role of ctILC2s in anti-tumor immunity in CRC and other cancer
297 indications.

298 We identified an additional helper-like ILC1 subset, named ctILC1-like TIGIT⁺, present in tumors
299 from CRC patients, but absent from the blood. ctILC1-like TIGIT⁺ had a transcriptional profile
300 more closely resembling the ILC1 gene signature than that of any other ILCs, but they segregated
301 away from ctILC1, suggesting that they differed markedly from ‘conventional’ gut ctILC1. ILC1-
302 like cells known as ‘intermediate ILC1s’ (intILC1s) have also been described in a mouse model of
303 methylcholanthrene (MCA)-induced tumors ⁴⁷. In humans, CD56⁺CD16⁻ ILC1-like cells have
304 been found in solid tumors and in peritoneal and pleural fluids from cancer patients ⁴⁸, and the
305 cytotoxic functions of these cells are altered in the peripheral blood of donors with acute myeloid
306 leukemia ⁴⁹. Intratumoral intILC1 may emerge from NK cell differentiation driven by TGF- β
307 signaling, a phenomenon known as ILC plasticity ^{47, 50}. The conversion of ILC3s into ILC1s upon
308 TGF- β signaling has been demonstrated in humanized mice and a transitional ILC3-ILC1
309 population has been identified in the human intestine ⁴⁰. We observed no such phenomenon in our

310 gut ILC dataset and none of the algorithms tested was able to establish a relatedness between
311 ctILC1-like TIGIT⁺ and another gut ILC subset reflecting possible differentiation (data not shown).
312 The mechanisms by which ctILC1-like TIGIT⁺ emerge in CRC tumors thus remain to be
313 determined. We observed a plasticity of ILC1 towards ILC3 in the blood of CRC patients, but not
314 in healthy donors, suggesting the presence of soluble signals driving ILC1-ILC3 plasticity, such as
315 sustained IL-23 levels ⁵¹. The biological relevance of such ILC1-ILC3 plasticity in the blood of
316 CRC patients is not clear.

317 intILC1s and ILC1s produced large amounts of TNF- α and were found to be ineffective at
318 controlling carcinogenesis, potentially even promoting metastasis in mouse models ⁴⁷. In human,
319 CD56⁺CD16⁻ ILC1-like cells express the pro-angiogenic factor VEGF, which may also favor
320 tumor growth ⁴⁸. In CRC patients, the frequency of ILC1s has been shown to be higher in tumor
321 tissues than in the normal mucosa ^{28, 29}, and to increase, at the expense of ILC3s, with tumor
322 progression ²⁹. These results suggest that high ILC1 levels may be predictive of a poor prognosis
323 in cancer. The issue of the specific biological function of the ctILC1-like subset relative to
324 classical TILC1 in CRC tumors also needs to be addressed, because ctILC1-like cells have high
325 levels of PD1 and TIGIT, and may be further unleashed by anti-PD1 and anti-TIGIT
326 immunotherapies.

327 We characterized the levels of three subsets: ILC3, ILC3/NK and ILC1, in the normal mucosa of
328 all donors. A donor-specific effect was observed in the ILC3 subsets, suggesting possible ILC3-
329 imprinting by the microbiota. This effect was absent in blood ILC3 population from healthy
330 donors, which was similar to CRC patient blood. Thus, alteration of gut-microbiota did not **seem**
331 to influence ILC3 population in the blood. One explanation could reside in the fact that ILC3 are
332 largely resident in tissues ⁵². Interestingly, CRC tumors had much lower levels of ILC3s and

333 displayed a loss of this apparent donor specificity. CRC is frequently associated with tumor
334 dysbiosis, involving massive changes to the composition of the microbiota⁵³⁻⁵⁷. ILC3s are major
335 regulators of intestinal barrier integrity and immune homeostasis. It might therefore be beneficial
336 to promote both ILC3 recolonization and diversification in CRC patients. ILC3 heterogeneity
337 could potentially be boosted by increasing microbial diversity.

338 We also defined a population of ILC3/NK cells in healthy gut mucosa. These cells had
339 transcriptomic features in common with both ILC3 and NK cells. They differ from ILC3s mostly
340 in terms of their *NKG7*, *KLRD1* (CD94), *GZMK*, *XCL2* and *CCL4* expression. The
341 biological role of this ILC3/NK subset and its relatedness to ‘classical’ ILC3 remain to be
342 addressed.

343 A recent study in a mouse model of CRC confirmed the diversity of ILC populations present
344 within the tumor⁴⁶. The authors identified 6 subsets of helper ILC encompassing 1 ILC1, 3 ILC2
345 (A, B and C), 1 ILC3 and 1 ‘ILCreg’. This study also presented results obtained by flow
346 cytometry in human colorectal tumors that corroborated the presence of PD1⁺ ILC2 and ILCreg
347 in patients with advanced CRC. We did not find these populations in our study, which is based
348 on the analysis of donors with early stage disease. However, these results suggest the need for an
349 additional comparative scRNAseq study to understand the evolution of the heterogeneity of
350 helper-like ILC as the disease progresses.

351 SLAMF1 was the only cell surface marker for which transcript levels were higher in ctILCs and
352 blood ILCs from CRC patients. ILCs expressing SLAMF1 on their surface were also present at
353 higher frequency in tumors and blood from CRC patients than in healthy donors. SLAMF1 is a
354 single-chain type I transmembrane receptor bearing two immunoreceptor tyrosine-based switch
355 motifs (ITSM) in its cytoplasmic tail, thus recruiting Src homology 2 (SH2) domain-containing

356 signal transduction molecules like SLAM-associated protein (SAP) to initiate downstream
357 signaling cascades ^{38, 58, 59}. SLAMF1 is a self-ligand but also a microbial receptor for
358 morbilliviruses and a bacterial sensor involved in the elimination of Gram-negative bacteria ^{38, 60-}
359 ⁶². SLAMF1 is expressed by almost all hematopoietic cells except NK cells, particularly those
360 with an activated phenotype, and is upregulated upon cell activation ^{38, 63}. A large proportion of
361 ILCs in the bloodstream expressed SLAMF1 on their surface at steady state, but no such
362 expression was observed on ILCs from normal gut mucosa. By contrast, SLAMF1 was expressed
363 on ctILCs from CRC patients, suggesting that ctILCs may be more activated in the tumor bed
364 than in the normal adjacent mucosa. Nevertheless, the effect of SLAMF1 engagement at the cell
365 surface of helper-like ILCs on the biology of these cells remains to be investigated. High levels
366 of SLAMF1 were correlated with better survival of CRC patients. Our results therefore suggest
367 that SLAMF1 is an anti-tumor biomarker in CRC.

368 ILCs have emerged as tissue-specific modulators of cancer immunity that can control various
369 aspects of immunotherapy. As ILCs and T cells co-exist in human cancers and have stimulatory
370 and inhibitory pathways in common, immunotherapy strategies targeting anti-cancer ILCs may be
371 as important as strategies targeting T cells. Our results suggest that ILCs are part of the tumor
372 microenvironment, as subsets of ctILCs are present in CRC. It is tempting to speculate that they
373 may regulate immunity at the tumor bed or have a direct effect on tumor cells. Further studies are
374 required to determine whether it is possible to define more tumor-specific subsets differing in
375 terms of activation status, with either pro- or anti-tumor immunity effects, in cancers arising in
376 different tissues.

377

378 **Limitations of the Study**

379 This study mainly used the scRNAseq technology to decipher the heterogeneity of ILCs in healthy
380 donor and CRC patients. We did not found ILC2s in normal mucosa by scRNAseq but in tumors.
381 The mechanisms involved in the recruitment/differentiation of ILC2s in CRC tumors remain to be
382 investigated. The functions of tumor-specific ILC1-like cells and *SLMAFI*⁺ ILCs have not been
383 addressed in this first study.

384

385 **Acknowledgments**

386 This work was supported by grants from the National Natural Science Foundation of China (No.
387 31930035, 91942311, and 81971487) and Shanghai Science and Technology Commission
388 (20JC1410100).

389 **Author contributions**

390 Conceptualization, J.Q., A.C., E.V., and B.S.; Investigation, J.Q., A.C.; Formal Analysis, J.Q.,
391 A.C. B.E., Y.Y., and L.B.; Validation, J.Q.; Resources, Z.W., T.Z, L.H., Y.L., H.L., N.W., M.Z.,
392 L.C.; Writing – Original Draft, J.Q., A.C., L.S., Y.Y., B.S., E.N.M., E.V.; Writing –Review &
393 Editing, J.Q., A.C., L.S., B.S., E.N.M., E.V.; Funding Acquisition, L.S., and B.S.; Supervision,
394 L.S., E.N.M., E.V., and B.S.

395

396 **Declaration of Interests**

397 Eric Vivier is Innate Pharma employee. The others authors declare no competing interests.
398 Patents related to this work were under application.

399

400 **Main figure tiles and figure legends**

401 **Figure 1. scRNAseq analysis reveals the presence of ILC1s, ILC3s and ILC3/NKs, but not**
402 **ILC2s, in normal mucosa.**

403 (A) Uniform manifold approximation and projection (UMAP) plot of 16,145 ILCs from normal
404 mucosa from four patients. Cells are color-coded according to the defined subset. (B) UMAP with
405 color coding according to donor origin. (C) Unsupervised hierarchical clustering of the 6 clusters
406 from each donor based on mean expression levels for genes with variable expression within cells.
407 Samples are color-coded according to their relatedness to a particular subset. (D) Heatmap of the
408 542 genes (256 in nmC0-3, 97 in nmC4, 189 in nmC5) tested with a Wilcoxon rank-sum test
409 distinguishing the three groups of ILCs in normal mucosa. Cells are plotted in columns and genes
410 are shown in rows and ranked by adjusted p value < 0.05 . Gene expression is color-coded with a
411 scale based on z -score distribution from -2.5 (purple) to 2.5 (yellow). Squares identify specific
412 transcriptomic signatures of ILC subsets. (E) Principal component analysis (PCA) on the 3 groups
413 of ILC clusters of each sample based on the mean level of expression for genes with variable
414 expression. (F) Driving genes for each cell subset, accounting for 20% of the total information in
415 each PC from (E). (G) Top 10 expressed genes from the total gene set, and top 10 expressed genes
416 encoding transcription factors, secreted proteins and cell membrane markers significantly
417 differentiating between the groups of ILCs. Gene symbols and annotations were retrieved from
418 public databases. Transcription factor genes are color-coded in red, secreted protein genes in
419 orange, cell membrane protein genes in blue, and other protein-encoding genes in black. Genes
420 encoded both secreted and cell membrane proteins are color-coded in violet. Genes are ranked by
421 p -value. (H) Module score for tonsil ILC gene expression programs for each of the 3 groups of
422 ILCs, at the single-cell level. Kruskal-Wallis with Dunn's multiple-comparison tests were

423 performed with Benjamini-Hochberg adjusted p -values. Each comparison was statistically
424 significant and values are shown in Supplementary Table 3.

425

426 **Figure 2. scRNA-seq analysis reveals tumor-specific ILC1 and ILC2 subsets in CRC tissues.**

427 (A) UMAP plot of 15,101 CRC tissue ILCs (ctILCs) from the CRC tissues of 4 patients. Cells
428 are color-coded according to the defined subset. (B) UMAP with color coding for donor origin.

429 (C) Unsupervised hierarchical clustering of the 4 clusters from each donor based on mean
430 expression levels for genes with variable expression. (D) Heatmap of the 982 genes (463 in ctC0,

431 100 in ctC1, 314 in ctC2, 105 in ctC3) tested with a Wilcoxon rank-sum test distinguishing
432 between the 4 ctILC subsets in tumor tissue. Cells are plotted in columns and genes are shown in

433 rows and ranked by adjusted p values (< 0.05). Gene expression is color-coded with a scale
434 based on z -score distribution from -2.5 (purple) to 2.5 (yellow). Squares identify specific

435 transcriptomic signatures of ctILC subsets. (E) Principal component analysis (PCA) on the 4
436 ctILC subsets of each sample based on the mean level of expression of genes with variable

437 expression. (F) Driving genes for each cell subset accounting for 20% of the total information in
438 each PC from (E). (G) Top 10 expressed genes from the total gene set, and top 10 expressed

439 genes encoding transcription factors, secreted proteins and cell membrane markers significantly
440 differentiating between the groups of ctILCs. Gene symbols and annotations were retrieved from

441 public databases. Transcription factor genes are color-coded in red, secreted protein genes in
442 orange, cell membrane protein genes in blue and other protein-encoding genes in black. Genes

443 encoded both secreted and cell membrane proteins are color-coded in violet. Genes are ranked by
444 p -value. (H) Module score for tonsil ILC gene expression programs, at the single-cell level, for

445 each of the 4 ctILCs subsets. Kruskal-Wallis with Dunn's multiple-comparison tests were

446 performed with Benjamini-Hochberg adjusted p values. Each comparison was statistically
447 significant and values are shown in Supplementary Table 3.

448

449 **Figure 3. Characterization of tumor tissue-specific ILC subsets.**

450 (A) UMAP plot of 41,603 ILCs from normal blood, CRC blood and CRC tissue. Cells are color-
451 coded according to the defined subset. (B) Unsupervised hierarchical clustering of normal blood,
452 CRC blood and CRC tissue ILCs from each donor, based on the mean level of expression of genes
453 with variable expression. (C) Heatmap of the 899 genes (44 in normal blood, 70 in CRC blood,
454 775 in CRC tissue) tested in a Wilcoxon rank-sum test distinguishing between the three organs.
455 Cells are plotted in columns and genes are shown in rows and ranked by adjusted p values (< 0.05).
456 Gene expression is color-coded with a scale based on z -score distribution from -2.5 (purple) to 2.5
457 (yellow). Squares identify specific transcriptomic signatures of ILC subsets. (D) Unsupervised
458 hierarchical clustering of normal blood ILCs (nbILCs), CRC blood ILCs (cbILCs) and CRC tissue
459 ILCs (ctILCs) from each donor, at the subset level, based on the mean expression level for genes
460 with variable expression. (E) Venn diagram representing the intersection between the gene
461 signatures of the 4 ILC1 subsets from normal blood, CRC blood, normal mucosa, and CRC tissue.
462 (F) Venn diagram representing the intersection between the gene signatures of the 3 ILC2 subsets
463 from normal blood, CRC blood, and CRC tissue.

464

465 **Figure 4. Specific gene signature of ILC in CRC.**

466 (A) UMAP plot of 31,246 ILCs from normal mucosa and CRC tissue. Cells are color-coded
467 according to the defined subset. (B) Unsupervised hierarchical clustering of normal mucosa and
468 CRC tissue ILCs from each donor based on the mean level of expression for genes with variable

469 expression. (C) Heatmap of the 331 genes (266 in CRC tumor, 51 in normal mucosa) tested with
470 a Wilcoxon rank-sum test distinguishing between the two organs. Cells are plotted in columns
471 and genes are shown in rows and ranked by adjusted p value (< 0.05). Gene expression is color-
472 coded with a scale based on z -score distribution from -2.5 (purple) to 2.5 (yellow). Squares
473 identify specific transcriptomic signatures of ILC subsets. (D) UMAP plot of 26,502 ILCs from
474 normal blood and CRC blood. Cells are color-coded according to the defined subsets. (E)
475 Unsupervised hierarchical clustering of normal blood and CRC blood ILCs from each donor,
476 based on the mean level of expression of genes with variable expression. (F) Heatmap of the 254
477 genes (233 in CRC blood, 23 in normal blood) tested with a Wilcoxon rank sum test
478 distinguishing between the 2 organs. Cells are plotted in columns and genes are shown in rows
479 and ranked by adjusted p value (< 0.05). Gene expression is color-coded with a scale based on z -
480 score distribution from -2.5 (purple) to 2.5 (yellow). Squares identify specific transcriptomic
481 signatures of ILC subsets. (G) Venn diagram representing the intersection of gene signatures
482 between normal blood and CRC blood, and between normal mucosa and CRC tissue. (H) Feature
483 plots of relative levels of *SLAMF1* expression on each of the ILCs from normal blood, CRC
484 blood, normal mucosa, and tumor tissue. (I) Feature plots of the relative expression levels of
485 *AQP3*, *HPGD*, *TLE4* and *PRDM1* in normal blood, blood from CRC patients, normal mucosa
486 and tumor tissue.

487

488 **Figure 5. SLAMF1 is a biomarker in CRC.**

489 (A) Representative flow cytometry profile of TIGIT cell surface expression on the ctILC1-like
490 subset. (B) Flow cytometry analysis of ILC subsets from normal mucosa ($n=8-16$) and CRC
491 tissues ($n=7-16$). Data show the frequencies of the indicated subset among total ILCs. (C)

492 Kaplan-Meier curves of overall survival stratified by IL-33 expression in CRC patients from
493 TCGA. The optimal cut-off for patient stratification was obtained with a Cox proportional
494 hazards model and the *p*-value was calculated in a log-rank test. IL-33-high group (*n*=369); IL-
495 33-low group (*n*=84). **(D)** Flow cytometry analysis of blood ILC subsets from healthy donors
496 (*n*=18) and CRC patients (*n*=16). **(E)** Representative FACS profile of SLAMF1 cell surface
497 expression on ILCs. **(F)** Flow cytometry analysis of SLAMF1 expression on total ILCs from
498 normal mucosa (*n*=7) and CRC tissues (*n*=7). The data show frequencies of SLAMF1⁺ cells
499 among total ILCs. **g**, Flow cytometry analysis of SLAMF1 expression on total blood ILCs from
500 healthy donors (*n*=14) and CRC patients (*n*=5). Data show frequencies of SLAMF1⁺ cells among
501 total ILCs. **(H)** Differentially expressed (DE) genes between *SLAMF1*⁺ ILCs and *SLAMF1*⁻ ILCs
502 in CRC tissues. The DE transcriptional factors and cytokines are labeled by red and orange text,
503 respectively. Red dots mean genes up-regulated in *SLAMF1*⁺ ILCs, and blue dots represent genes
504 up-regulated in *SLAMF1*⁻ ILCs. Kaplan-Meier curves for overall survival stratified by SLAMF1
505 expression level in colon **(I)** and rectum **(J)** cancer patients from TCGA. The optimal cut-off for
506 patient stratification was obtained with a Cox proportional hazards model and the *p*-value was
507 calculated in a log-rank test. In **(I)**, *SLAMF1*-high group (*n*=393); *SLAMF1*-low group (*n*=60). In
508 **(J)**, *SLAMF1*-high group (*n*=119); *SLAMF1*-low group (*n*=46).
509 In **(B)**, **(D)**, statistical significance was calculated in Kruskal-Wallis tests with Dunn's multiple
510 comparison tests, and *p*-values were adjusted with the Benjamini-Hochberg method. In **(F)**, **(G)**,
511 Mann-Whitney tests of unpaired nonparametric *t* tests were used. In **(H)**, statistical analysis is
512 performed by Wilcoxon test.

513 **p*-value<0.05; ***p*-value<0.01; ****p*-value<0.001; *****p*-value<0.0001.

514 **STAR Methods**

515 **RESOURCE AVAILABILITY**

516 **Lead Contact**

517 Further information and resource requests should be directed to and will be fulfilled by the Lead
518 Contact, Bing Su (bingsu@sjtu.edu.cn).

519 **Materials Availability**

520 This study did not generate new materials.

521 **Data and Code Availability**

522 Raw sequence data of each sample is available to download at Genome Sequence Archive for
523 Human, GSA-Human (Accession number, HRA000919).

524 **EXPERIMENTAL MODEL AND SUBJECT DETAILS**

525 Clinical samples were obtained from colorectal cancer (CRC) patients without chemo-radiation
526 therapy before resection of the tumor and healthy individuals who gave informed consent, after
527 approval had been obtained from the local medical ethics committee of Ruijin Hospital and
528 Xinhua Hospital Affiliated to Shanghai Jiao Tong University School of Medicine. Four CRC
529 patients were recruited for scRNAseq at diagnosis (Table S1). Adjacent tissue (normal mucosa),
530 and CRC tissue were collected from these four CRC donors whereas blood samples were collected
531 except P4. Healthy blood for scRNAseq were recruited from individuals undergoing routine
532 colonoscopy who were generally in good health, with no other relevant medical history, such as
533 inflammatory bowel disease (IBD) or CRC (Table S1).

534 **METHOD DETAILS**

535 **Isolation of human lymphocytes**

536 Fresh intestine tissues were quickly placed into 50 mL tubes containing RPMI 1640 medium plus
537 10% FBS, and were transported on ice to laboratory for cell preparation usually within 2 hours.
538 Adipose tissue and visible blood vessels were removed from the tissue manually. Specimens were
539 weighed and washed with PBS and then cut into small pieces. Normal tissue was incubated with
540 10 mL freshly prepared intraepithelial lymphocyte solution (5 mM EDTA, 15 mM HEPES, 10%
541 FBS, 1 mM DTT in PBS), for 1 hour at 37°C, with shaking at 200 rpm. CRC tissue was washed
542 with 10 mL freshly prepared 6.5 mM DTT in PBS for 15 min at 37°C, with shaking. After
543 incubation, the tissue pieces were rinsed twice with PBS and subjected to enzymatic digestion for
544 1 hour at 37°C, with shaking (0.38 mg/mL collagenase VIII, 0.1 mg/mL DNase I, 100 U/ml
545 penicillin, 100 mg/mL streptomycin, 10% FBS in RPMI 1640 medium). The digested tissues were
546 then shaken vigorously by hand for 5 min and mechanically dissociated with a 21-gauge syringe.
547 The resulting cell suspension was filtered through a cell strainer with 100 µm pores into a new 50
548 mL conical tube, and PBS was added to a final volume of 30 mL. Cells were then centrifuged at
549 1,800 rpm for 5 min. The supernatants were discarded and the cell pellets were resuspended in
550 RPMI 1640 medium supplemented with 10% FBS. Cells were centrifuged on a Ficoll gradient and
551 then washed with PBS before use.

552 Peripheral blood mononuclear cells (PBMCs) were obtained from human blood samples
553 centrifuged on a Ficoll gradient. Briefly, blood was mixed with an equal volume of 2% FBS in
554 PBS and gently layered on the Ficoll gradient. Cells were centrifuged at 1000 x g for 25 min,
555 without braking. The cells in the middle layer were then washed once with PBS and resuspended
556 in 2% FBS in PBS for use.

557

558 **Sorting of ILCs**

559 Freshly prepared human cells were resuspended in PBS and incubated with a live/dead cell marker,
560 Fixable Viability stain 520 (BD 564407), for 10 min at 4°C. Cells were washed and suspended in
561 2% FBS, 2 mM EDTA in PBS (FACS buffer), supplemented with 10% mouse serum and 40%
562 Brilliant Strain Buffer. Cells were first stained with 1:50 human Fc Block for 10 min at 4°C and
563 then incubated with antibodies directed against CD45, CD127, CD117, CRTH2, and against
564 lineage markers (TCR $\gamma\delta$, TCR $\alpha\beta$, CD3, CD19, CD14, CD16, CD94, CD123, CD34, CD303 and
565 Fc ϵ RI) for 30 min at room temperature. Human cells were washed with FACS buffer, centrifuged
566 and resuspended in FACS buffer. Live ILCs in RPMI 1640 supplemented with 20% FBS were
567 sorted in a BD FACSAria III cell sorter (BD Biosciences).

568

569 **Flow cytometry for ILCs**

570 For cell surface staining of ILCs, freshly prepared human cells were stained with live/dead cell
571 markers, Fixable Viability stain 520 (BD 564407), and Fc Block as for ILCs sorting. Cells were
572 stained with surface antibodies against CD45, CD127, CD117, CRTH2, CD5, TIGIT and
573 SLAMF1 and antibodies against same lineage markers for ILCs sorting for 30 min at room
574 temperature. For each of the staining, paired samples from same patients were used. PBMC from
575 more healthy donors was stained at same time. Cells were kept at 4°C and analyzed on a BD
576 Symphony (BD Biosciences). Flow data was analyzed with FlowJo software (FlowJo LLC).
577 Statistical analysis was performed by Mann-Whitney tests of unpaired nonparametric *t* tests or
578 Kruskal-Wallis tests with Dunn's multiple comparison tests. *p*-values were adjusted with the
579 Benjamini-Hochberg method for multiple comparison tests. * *p*-value < 0.05, ** *p*-value < 0.01,
580 *** *p*-value < 0.001, **** *p*-value < 0.0001.

581

582 **Single-cell RNA sequencing**

583 Purified ILCs were resuspended in PBS supplemented with 0.04% BSA, and kept on ice. Cells
584 were counted and cell density was adjusted to that recommended for 10x Genomics Chromium
585 single-cell 3' v3 processing and library preparation. Sequencing was performed on an Illumina
586 platform (NovaSeq 6000), by GENERGY BIO (Shanghai, China), at a sequencing depth of about
587 90,000 reads per single cell.

588

589 **Raw 10X read alignment, quality control and normalization**

590 Raw sequencing reads were subjected to quality control with FastQC software v0.11.9
591 (<https://www.bioinformatics.babraham.ac.uk/projects/fastqc/>). Sequencing data in a bcl file were
592 converted to FASTQ format with Illumina bcl2fastq2 Conversion Software v2.20
593 (<https://support.illumina.com/downloads/bcl2fastq-conversion-software-v2-20.html>). We then
594 used Cell Ranger Single Cell Software Suite v. 2.2 to process, align, and summarize unique
595 molecular identifier (UMI) counts, according to the standard pipeline and default parameters
596 described at [https://support.10xgenomics.com/single-cell-gene-expression/software/pipelines](https://support.10xgenomics.com/single-cell-gene-expression/software/pipelines/latest/)
597 [/latest/](https://support.10xgenomics.com/single-cell-gene-expression/software/pipelines/latest/). Briefly, we used the standard Cell Ranger Count pipeline to align FASTQ reads with the
598 GRch38 genome. We then filtered sequencing reads on the basis of base-calling quality scores,
599 and assigned cell barcodes and UMIs to each read. The Cell Ranger aggr pipeline was used to
600 normalize all scRNAseq data with default parameters, to obtain a uniform sequencing depth. The
601 combined feature-barcode matrix was used for downstream analysis.

602 During quality control with Seurat analysis, raw UMI count matrices were filtered to remove
603 genes expressed in fewer than three cells, cells with fewer than 200 genes, cells with more than

604 4000 genes, and cells with high percentages of mitochondrial genes (more than 8%). The resulting
605 matrix was then normalized by a global-scaling method, converted with a scaling factor (10,000
606 by default) and log-transformed with the “LogNormalize” function in Seurat for downstream
607 analysis.

608

609 **Filtering contaminated cells**

610 We used the R package SingleR ⁶⁷ and default parameters to assign individual cells to cell types,
611 with the Human Primary Cell Atlas Data as the reference dataset. Each single cell was annotated
612 with a cell type in “label.main” of the dataset. As the dataset did not include the human ILC
613 dataset, and, given the similarities between ILCs and T cells or NK cells, we retained cells labeled
614 as both NK and T cells. We removed cells considered as doublets with an range from 0.14% to
615 3.69%. In addition, when analyzing the ILC3 in tumor tissue, two small clusters with percentage
616 ranging from 0.35% to 3.59% that were not present in each donor were removed. Donor-specific
617 clusters with a strong specific NK cell signature were considered to be true NK cell contaminants
618 and were removed from downstream analysis.

619

620 **Reduction of the number of dimensions and clustering**

621 The top 2000 variable genes were selected with the “FindVariableGenes” function of Seurat ⁶⁸ and
622 used for principal component analysis (PCA). For ILCs in normal mucosa, we retained the first 40
623 PCs. For normal blood, CRC blood and tumor tissue, we retained the top 20 PCs. Clusters were
624 identified with the “FindClusters” function, with the algorithm based on the optimization of
625 nearest-neighbor modularity implemented in Seurat and visualized with the uniform manifold

626 approximation and projection (UMAP) algorithm. For comparisons of different tissues, the “merge”
627 function was used to pool the individual Seurat objects. For donor and tissue data visualization,
628 the “group.by” parameters were set as intended information when plotting with “DimPlot”
629 function in Seurat.

630

631 **Batch effect correction for ILC3 subsets in normal and tumor mucosa**

632 ILC3 clusters in tumor tissue and both ILC3 and ILC3/NK clusters in normal mucosa were
633 subsampled for downstream clustering. The batch effect was corrected with the “IntegrateData”
634 function of the standard workflow of Seurat, based on previously identified anchors (Butler et al.,
635 2018).

636

637 **Unsupervised hierarchical clustering**

638 Mean gene expression was analyzed for single cells in each cluster. Only genes previously shown
639 to display variable expression were used. We used the Heatmap.plus package to plot the
640 unsupervised clustering map. The Euclidean distance was calculated for genes in all clusters. For
641 normal mucosa, only the major donor-derived ILCs for cluster 0-4 were used for analysis.

642

643 **Principal component analysis**

644 Principal component analysis (PCA) was performed on the mean level of expression of variable
645 genes in clusters. The top 20 genes contributing to PC1 and PC2 or PC1 and PC3 were plotted.
646 For the analysis of ILCs in normal mucosa, we removed ILCs from donors other than the major
647 source of cluster 0-4. PCA gene loadings for the PCs corresponded to the 20 genes making the

648 largest contribution to the total amount of information represented by PC1 and PC2 or PC1 and
649 PC3.

650

651 **Differential expression analysis**

652 We used the “FindAllMarkers” function in Seurat to identify genes differentially expressed
653 between samples, for each cluster. The non-parametric Wilcoxon rank-sum test was used to obtain
654 *p*-values for comparisons, and the adjusted *p*-values, based on Bonferroni correction, for all genes
655 in the dataset. We used the following parameters for the calculation of log fold-change (logFC) in
656 expression values and to obtain *p*-values for all the variable genes for each cluster: min.pct = 0.05,
657 min.diff.pct = 0.1, logfc.threshold = 0.25. The log-transformed and scaled expression values of the
658 genes were used to generate a heatmap.

659

660 **Gene annotations**

661 Genes encoding transcription factors (TFs) were retrieved from four TF-related public datasets:
662 JASPAR⁶⁹ (<http://jaspar.genereg.net/>), DBD⁷⁰ (<http://www.transcriptionfactor.org/>),
663 AnimalTFDB⁷¹ (<http://bioinfo.life.hust.edu.cn/AnimalTFDB/>), and TF2DNA⁷²
664 (http://www.fiserlab.org/tf2dna_db/). Genes encoding cell membrane and secreted proteins were
665 obtained from The Human Protein Atlas⁷³
666 (<https://www.proteinatlas.org/humanproteome/tissue/secretome>). Genes were ranked by the
667 adjusted *p*-value for each ILCs cluster in tissue. The top 10 genes within each category (TF, cell
668 membrane, or secreted protein) was selected based on their original adjusted *p*-value in each
669 cluster.

670

671 **RNA velocity estimation**

672 We analyzed expression dynamics, using scRNA-seq data, by estimating the RNA velocities of
673 single cells by distinguishing between unspliced and spliced transcripts on the basis of the
674 previously aligned bam files of scRNA-seq data. The RNA velocity values for each gene in each
675 cell and the embedding of RNA velocity vectors in a low-dimension space were calculated with
676 the R package `velocity`.R⁷⁴ (<https://github.com/velocyto-team/velocyto.R>). RNA velocities were
677 then visualized on the UMAP projection by Gaussian smoothing on a regular grid.

678

679 **Scoring samples for ILC signatures**

680 ILC and NK cell signatures from tonsil tissue were defined by Björklund et al.,³¹. ILC1 and ILC3
681 signatures from jejunum, and ILC2 signatures from spleen were obtained from Yudanin et al.,³⁷.
682 Module scores were calculated with “AddModuleScore” in Seurat, for each ILC. Briefly, the mean
683 level of gene expression in a single cell was calculated, and the aggregate expression of control
684 feature sets was then subtracted from it. The control features were selected at random from all
685 features. For the module scores of ILC3 subsets from normal mucosa, the differentially expressed
686 gene signatures for each ILC3 subset were used, at single-cell level, on each ILC3 subset in CRC
687 tissues. Violin plots were used to visualize the module scores of each cluster.

688

689 **TCGA analysis**

690 RNAseq data from primary tumors and clinical annotations were downloaded using the package
691 TCGAbiolinks in September 2019. Kaplan-Meier curves were plotted using the R package

692 survminer. In order to split the expression levels in two groups, the cut-off which gave the lowest
693 p-value was used. Optimal cut-off for patient stratification was obtained with a Cox proportional
694 hazards model and p-value indicated in the plot was calculated with a log-Rank test.

695 **Quantification and statistical analysis**

696 Data are presented as the mean \pm standard error of the means (SEM), or standard deviations (SD).
697 GraphPad Prism 6 was used for statistical analysis, two-sided Wilcoxon test and Mann–Whitney
698 test were used for unpaired data. Kruskal-Wallis tests with Dunn’s multiple comparison tests was
699 used for multiple comparisons. Kaplan–Meier survival data were analyzed using two-sided log-
700 rank test. p values <0.05 were considered significantly statistical difference.

701 **SUPPLEMENTARY FILES**

702 Table S1. Clinical characteristics of CRC patients and healthy blood donors analyzed by
703 scRNAseq, Related to STAR Methods.

704 Table S2. Gene signatures of each clusters, related to Figure 1, 2, 3, 4 and Figure S3, S4, S5.

705 Adjusted p-values for non-parametric Wilcoxon rank-sum tests are provided.

706 Table S3. Statistical analysis of the module score for each cluster, Related to Figure 1H, Figure
707 2H, Figure S2B, S3K, S4H and S5H.

708 Kruskal-Wallis with Dunn’s multiple-comparison tests were performed with Benjamini-
709 Hochberg adjusted p-values.

710 **References**

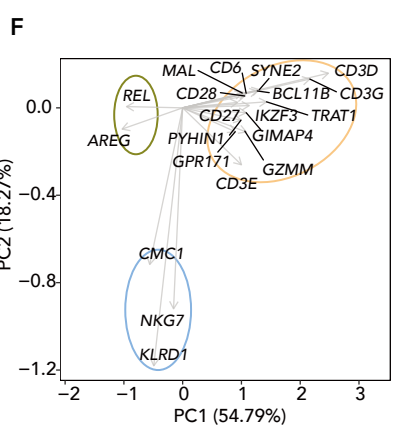
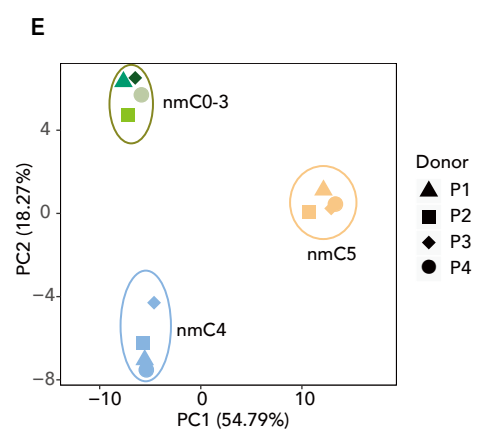
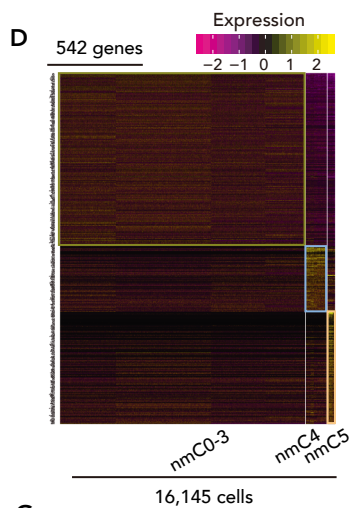
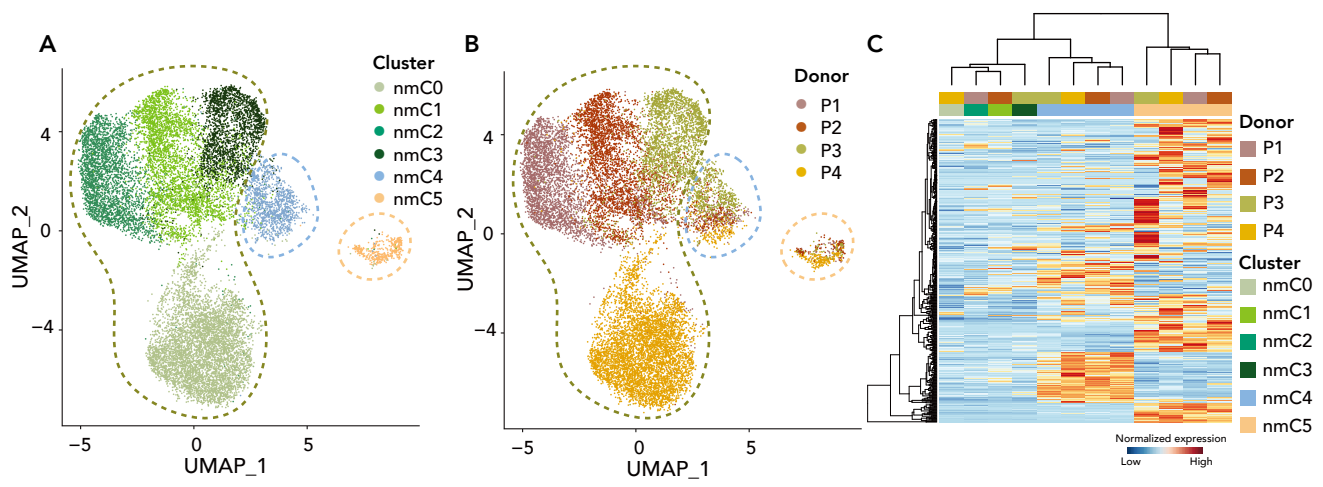
- 711 1. Baumeister SH, Freeman GJ, Dranoff G, Sharpe AH. Coinhibitory Pathways in
712 Immunotherapy for Cancer. *Annu Rev Immunol.* 2016;34:539-73.
- 713 2. Chen DS, Mellman I. Elements of cancer immunity and the cancer-immune set point.
714 *Nature.* 2017;541(7637):321-30.
- 715 3. Okazaki T, Chikuma S, Iwai Y, Fagarasan S, Honjo T. A rheostat for immune responses:
716 the unique properties of PD-1 and their advantages for clinical application. *Nat Immunol.*
717 2013;14(12):1212-8.
- 718 4. Schumacher TN, Schreiber RD. Neoantigens in cancer immunotherapy. *Science.*
719 2015;348(6230):69-74.
- 720 5. Sharma P, Allison JP. Immune checkpoint targeting in cancer therapy: toward
721 combination strategies with curative potential. *Cell.* 2015;161(2):205-14.
- 722 6. Okazaki T, Honjo T. PD-1 and PD-1 ligands: from discovery to clinical application. *Int*
723 *Immunol.* 2007;19(7):813-24.
- 724 7. Spits H, Artis D, Colonna M, Diefenbach A, Di Santo JP, Eberl G, et al. Innate lymphoid
725 cells--a proposal for uniform nomenclature. *Nature reviews Immunology.* 2013;13(2):145-9.
- 726 8. Vivier E, Artis D, Colonna M, Diefenbach A, Di Santo JP, Eberl G, et al. Innate Lymphoid
727 Cells: 10 Years On. *Cell.* 2018;174(5):1054-66.
- 728 9. Lopez-Soto A, Gonzalez S, Smyth MJ, Galluzzi L. Control of Metastasis by NK Cells.
729 *Cancer Cell.* 2017;32(2):135-54.
- 730 10. Chiossone L, Dumas PY, Vienne M, Vivier E. Natural killer cells and other innate
731 lymphoid cells in cancer. *Nat Rev Immunol.* 2018;18(11):671-88.
- 732 11. Castro F, Cardoso AP, Goncalves RM, Serre K, Oliveira MJ. Interferon-Gamma at the
733 Crossroads of Tumor Immune Surveillance or Evasion. *Front Immunol.* 2018;9:847.
- 734 12. Zaidi MR. The Interferon-Gamma Paradox in Cancer. *J Interferon Cytokine Res.*
735 2019;39(1):30-8.
- 736 13. Bie Q, Zhang P, Su Z, Zheng D, Ying X, Wu Y, et al. Polarization of ILC2s in peripheral
737 blood might contribute to immunosuppressive microenvironment in patients with gastric
738 cancer. *J Immunol Res.* 2014;2014:923135.
- 739 14. Trabanelli S, Chevalier MF, Martinez-Usatorre A, Gomez-Cadena A, Salome B, Lecciso M,
740 et al. Tumour-derived PGD2 and NKp30-B7H6 engagement drives an immunosuppressive ILC2-
741 MDSC axis. *Nat Commun.* 2017;8(1):593.
- 742 15. Chevalier MF, Trabanelli S, Racle J, Salome B, Cesson V, Gharbi D, et al. ILC2-modulated
743 T cell-to-MDSC balance is associated with bladder cancer recurrence. *J Clin Invest.*
744 2017;127(8):2916-29.
- 745 16. Saranchova I, Han J, Huang H, Fenninger F, Choi KB, Munro L, et al. Discovery of a
746 Metastatic Immune Escape Mechanism Initiated by the Loss of Expression of the Tumour
747 Biomarker Interleukin-33. *Sci Rep.* 2016;6:30555.
- 748 17. Ikitani M, Yanagibashi T, Ogasawara M, Tsuneyama K, Yamamoto S, Hattori Y, et al.
749 Identification of innate IL-5-producing cells and their role in lung eosinophil regulation and
750 antitumor immunity. *J Immunol.* 2012;188(2):703-13.

- 751 18. Kim J, Kim W, Moon UJ, Kim HJ, Choi HJ, Sin JI, et al. Intratumorally Establishing Type 2
752 Innate Lymphoid Cells Blocks Tumor Growth. *J Immunol*. 2016;196(5):2410-23.
- 753 19. Moral JA, Leung J, Rojas LA, Ruan J, Zhao J, Sethna Z, et al. ILC2s amplify PD-1 blockade
754 by activating tissue-specific cancer immunity. *Nature*. 2020;579(7797):130-5.
- 755 20. Eisenring M, vom Berg J, Kristiansen G, Saller E, Becher B. IL-12 initiates tumor rejection
756 via lymphoid tissue-inducer cells bearing the natural cytotoxicity receptor NKp46. *Nat Immunol*.
757 2010;11(11):1030-8.
- 758 21. Nussbaum K, Burkhard SH, Ohs I, Mair F, Klose CSN, Arnold SJ, et al. Tissue
759 microenvironment dictates the fate and tumor-suppressive function of type 3 ILCs. *J Exp Med*.
760 2017;214(8):2331-47.
- 761 22. Carrega P, Loiacono F, Di Carlo E, Scaramuccia A, Mora M, Conte R, et al. NCR(+)ILC3
762 concentrate in human lung cancer and associate with intratumoral lymphoid structures. *Nat*
763 *Commun*. 2015;6:8280.
- 764 23. Chan IH, Jain R, Tessmer MS, Gorman D, Mangadu R, Sathe M, et al. Interleukin-23 is
765 sufficient to induce rapid de novo gut tumorigenesis, independent of carcinogens, through
766 activation of innate lymphoid cells. *Mucosal Immunol*. 2014;7(4):842-56.
- 767 24. Kirchberger S, Royston DJ, Boulard O, Thornton E, Franchini F, Szabady RL, et al. Innate
768 lymphoid cells sustain colon cancer through production of interleukin-22 in a mouse model. *J*
769 *Exp Med*. 2013;210(5):917-31.
- 770 25. Bray F, Ferlay J, Soerjomataram I, Siegel RL, Torre LA, Jemal A. Global cancer statistics
771 2018: GLOBOCAN estimates of incidence and mortality worldwide for 36 cancers in 185
772 countries. *CA Cancer J Clin*. 2018;68(6):394-424.
- 773 26. Fuchs A, Vermi W, Lee JS, Lonardi S, Gilfillan S, Newberry RD, et al. Intraepithelial type 1
774 innate lymphoid cells are a unique subset of IL-12- and IL-15-responsive IFN-gamma-producing
775 cells. *Immunity*. 2013;38(4):769-81.
- 776 27. Simoni Y, Fehlings M, Kloverpris HN, McGovern N, Koo SL, Loh CY, et al. Human Innate
777 Lymphoid Cell Subsets Possess Tissue-Type Based Heterogeneity in Phenotype and Frequency.
778 *Immunity*. 2017;46(1):148-61.
- 779 28. Carrega P, Orecchia P, Quatrini L, Tumino N, Vene R, Benelli R, et al. Characterisation of
780 innate lymphoid cell subsets infiltrating colorectal carcinoma. *Gut*. 2020.
- 781 29. Ikeda A, Ogino T, Kayama H, Okuzaki D, Nishimura J, Fujino S, et al. Human NKp44+
782 group 3 innate lymphoid cells associate with tumor-associated tertiary lymphoid structures in
783 colorectal cancer. *Cancer Immunol Res*. 2020.
- 784 30. Gasteiger G, Fan X, Dikiy S, Lee SY, Rudensky AY. Tissue residency of innate lymphoid
785 cells in lymphoid and nonlymphoid organs. *Science*. 2015;350(6263):981-5.
- 786 31. Bjorklund AK, Forkel M, Picelli S, Konya V, Theorell J, Friberg D, et al. The heterogeneity
787 of human CD127(+) innate lymphoid cells revealed by single-cell RNA sequencing. *Nat Immunol*.
788 2016;17(4):451-60.
- 789 32. Grinberg-Bleyer Y, Oh H, Desrichard A, Bhatt DM, Caron R, Chan TA, et al. NF-kappa B c-
790 Rel Is Crucial for the Regulatory T Cell Immune Checkpoint in Cancer. *Cell*. 2017;170(6):1096-
791 108.
- 792 33. Victor AR, Nalin AP, Dong W, McClory S, Wei M, Mao C, et al. IL-18 Drives ILC3
793 Proliferation and Promotes IL-22 Production via NF-kappaB. *J Immunol*. 2017;199(7):2333-42.

- 794 34. Medley QG, Kedersha N, O'Brien S, Tian Q, Schlossman SF, Streuli M, et al.
795 Characterization of GMP-17, a granule membrane protein that moves to the plasma membrane
796 of natural killer cells following target cell recognition. *Proc Natl Acad Sci U S A*. 1996;93(2):685-
797 9.
- 798 35. Ercolano G, Wyss T, Salome B, Romero P, Trabanelli S, Jandus C. Distinct and shared
799 gene expression for human innate versus adaptive helper lymphoid cells. *J Leukoc Biol*. 2020.
- 800 36. Robinette ML, Fuchs A, Cortez VS, Lee JS, Wang Y, Durum SK, et al. Transcriptional
801 programs define molecular characteristics of innate lymphoid cell classes and subsets. *Nat*
802 *Immunol*. 2015;16(3):306-17.
- 803 37. Yudanin NA, Schmitz F, Flamar AL, Thome JJC, Tait Wojno E, Moeller JB, et al. Spatial and
804 Temporal Mapping of Human Innate Lymphoid Cells Reveals Elements of Tissue Specificity.
805 *Immunity*. 2019;50(2):505-19 e4.
- 806 38. Gordiienko I, Shlapatska L, Kovalevska L, Sidorenko SP. SLAMF1/CD150 in hematologic
807 malignancies: Silent marker or active player? *Clin Immunol*. 2019;204:14-22.
- 808 39. Hong JT, Son DJ, Lee CK, Yoon DY, Lee DH, Park MH. Interleukin 32, inflammation and
809 cancer. *Pharmacol Ther*. 2017;174:127-37.
- 810 40. Cella M, Gamini R, Secca C, Collins PL, Zhao S, Peng V, et al. Subsets of ILC3-ILC1-like
811 cells generate a diversity spectrum of innate lymphoid cells in human mucosal tissues. *Nat*
812 *Immunol*. 2019;20(8):980-91.
- 813 41. Trabanelli S, Gomez-Cadena A, Salome B, Michaud K, Mavilio D, Landis BN, et al. Human
814 innate lymphoid cells (ILCs): Toward a uniform immune-phenotyping. *Cytometry B Clin Cytom*.
815 2018;94(3):392-9.
- 816 42. Salimi M, Wang R, Yao X, Li X, Wang X, Hu Y, et al. Activated innate lymphoid cell
817 populations accumulate in human tumour tissues. *BMC Cancer*. 2018;18(1):341.
- 818 43. Wagner M, Ealey KN, Tetsu H, Kiniwa T, Motomura Y, Moro K, et al. Tumor-Derived
819 Lactic Acid Contributes to the Paucity of Intratumoral ILC2s. *Cell Rep*. 2020;30(8):2743-57 e5.
- 820 44. Cui G, Qi H, Gundersen MD, Yang H, Christiansen I, Sorbye SW, et al. Dynamics of the IL-
821 33/ST2 network in the progression of human colorectal adenoma to sporadic colorectal cancer.
822 *Cancer Immunol Immunother*. 2015;64(2):181-90.
- 823 45. Mertz KD, Mager LF, Wasmer MH, Thiesler T, Koelzer VH, Ruzzante G, et al. The IL-
824 33/ST2 pathway contributes to intestinal tumorigenesis in humans and mice. *Oncoimmunology*.
825 2016;5(1):e1062966.
- 826 46. Wang S, Qu Y, Xia P, Chen Y, Zhu X, Zhang J, et al. Transdifferentiation of tumor
827 infiltrating innate lymphoid cells during progression of colorectal cancer. *Cell Res*.
828 2020;30(7):610-22.
- 829 47. Gao Y, Souza-Fonseca-Guimaraes F, Bald T, Ng SS, Young A, Ngiow SF, et al. Tumor
830 immunoevasion by the conversion of effector NK cells into type 1 innate lymphoid cells. *Nat*
831 *Immunol*. 2017;18(9):1004-15.
- 832 48. Levi I, Amsalem H, Nissan A, Darash-Yahana M, Peretz T, Mandelboim O, et al.
833 Characterization of tumor infiltrating natural killer cell subset. *Oncotarget*. 2015;6(15):13835-
834 43.
- 835 49. Salome B, Gomez-Cadena A, Loyon R, Suffiotti M, Salvestrini V, Wyss T, et al. CD56 as a
836 marker of an ILC1-like population with NK cell properties that is functionally impaired in AML.
837 *Blood Adv*. 2019;3(22):3674-87.

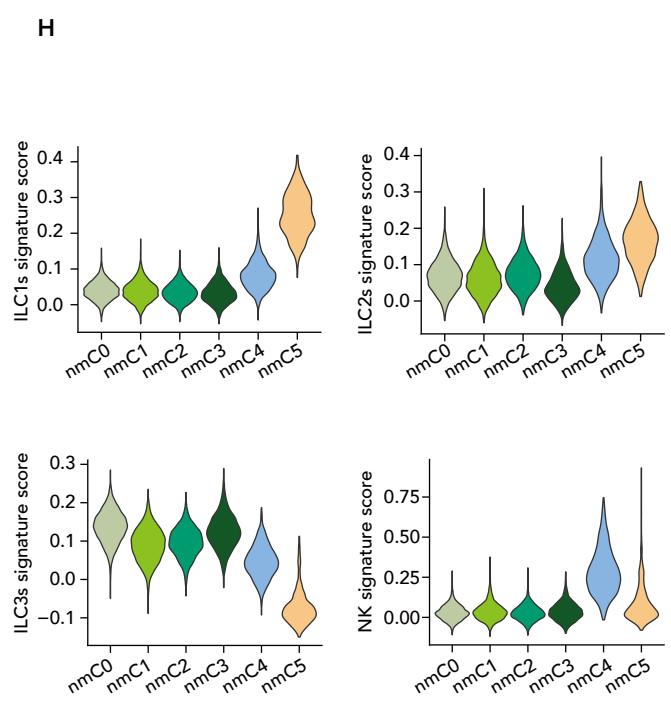
- 838 50. Cortez VS, Cervantes-Barragan L, Robinette ML, Bando JK, Wang Y, Geiger TL, et al.
839 Transforming Growth Factor-beta Signaling Guides the Differentiation of Innate Lymphoid Cells
840 in Salivary Glands. *Immunity*. 2016;44(5):1127-39.
- 841 51. Koh J, Kim HY, Lee Y, Park IK, Kang CH, Kim YT, et al. IL23-Producing Human Lung Cancer
842 Cells Promote Tumor Growth via Conversion of Innate Lymphoid Cell 1 (ILC1) into ILC3. *Clin*
843 *Cancer Res*. 2019;25(13):4026-37.
- 844 52. Dutton EE, Gajdasik DW, Willis C, Fiancette R, Bishop EL, Camelo A, et al. Peripheral
845 lymph nodes contain migratory and resident innate lymphoid cell populations. *Sci Immunol*.
846 2019;4(35).
- 847 53. Feng Q, Liang S, Jia H, Stadlmayr A, Tang L, Lan Z, et al. Gut microbiome development
848 along the colorectal adenoma-carcinoma sequence. *Nat Commun*. 2015;6:6528.
- 849 54. Liang Q, Chiu J, Chen Y, Huang Y, Higashimori A, Fang J, et al. Fecal Bacteria Act as Novel
850 Biomarkers for Noninvasive Diagnosis of Colorectal Cancer. *Clin Cancer Res*. 2017;23(8):2061-
851 70.
- 852 55. Nakatsu G, Li X, Zhou H, Sheng J, Wong SH, Wu WK, et al. Gut mucosal microbiome
853 across stages of colorectal carcinogenesis. *Nat Commun*. 2015;6:8727.
- 854 56. Yazici C, Wolf PG, Kim H, Cross TL, Vermillion K, Carroll T, et al. Race-dependent
855 association of sulfidogenic bacteria with colorectal cancer. *Gut*. 2017;66(11):1983-94.
- 856 57. Yu J, Feng Q, Wong SH, Zhang D, Liang QY, Qin Y, et al. Metagenomic analysis of faecal
857 microbiome as a tool towards targeted non-invasive biomarkers for colorectal cancer. *Gut*.
858 2017;66(1):70-8.
- 859 58. Vilar ML, Frutuoso MS, Arruda SM, Lima DM, Bezerra CS, Pompeu MM. The role of the
860 SLAM-SAP signaling pathway in the modulation of CD4+ T cell responses. *Braz J Med Biol Res*.
861 2011;44(4):276-82.
- 862 59. Romero X, Sintes J, Engel P. Role of SLAM family receptors and specific adapter SAP in
863 innate-like lymphocytes. *Crit Rev Immunol*. 2014;34(4):263-99.
- 864 60. Yurchenko M, Skjesol A, Ryan L, Richard GM, Kandasamy RK, Wang NH, et al. SLAMF1 is
865 required for TLR4-mediated TRAM-TRIF-dependent signaling in human macrophages. *J Cell Biol*.
866 2018;217(4):1411-29.
- 867 61. Berger SB, Romero X, Ma CY, Wang GX, Faubion WA, Liao GX, et al. SLAM is a microbial
868 sensor that regulates bacterial phagosome functions in macrophages. *Nature Immunology*.
869 2010;11(10):920-U70.
- 870 62. Song TF, Dong CS, Xiong SD. Signaling lymphocyte-activation molecule SLAMF1
871 augments mycobacteria BCG-induced inflammatory response and facilitates bacterial clearance.
872 *Int J Med Microbiol*. 2015;305(6):572-80.
- 873 63. Romero X, Benitez D, March S, Vilella R, Miralpeix M, Engel P. Differential expression of
874 SAP and EAT-2-binding leukocyte cell-surface molecules CD84, CD150 (SLAM), CD229 (Ly9) and
875 CD244 (2B4). *Tissue Antigens*. 2004;64(2):132-44.
- 876 64. Butler A, Hoffman P, Smibert P, Papalexi E, Satija R. Integrating single-cell transcriptomic
877 data across different conditions, technologies, and species. *Nat Biotechnol*. 2018;36(5):411-20.
- 878 65. Falcon S, Gentleman R. Using GOSTats to test gene lists for GO term association.
879 *Bioinformatics*. 2007;23(2):257-8.

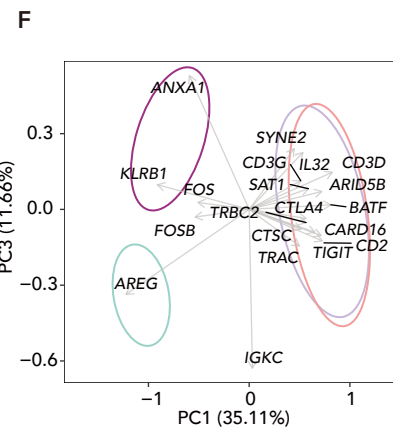
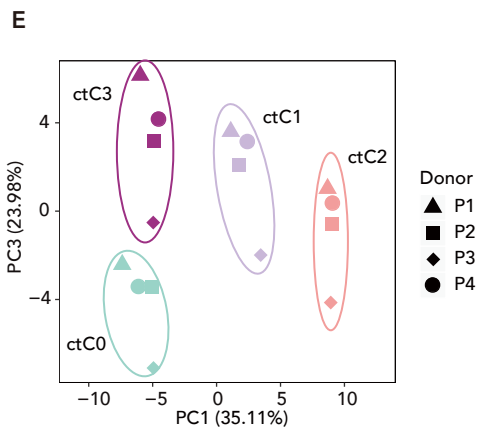
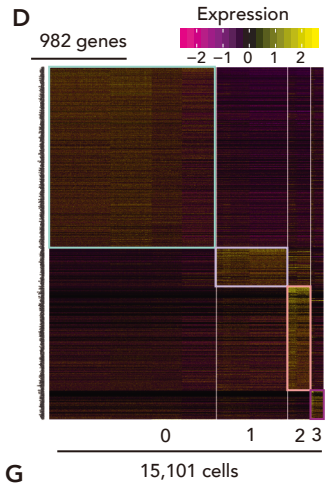
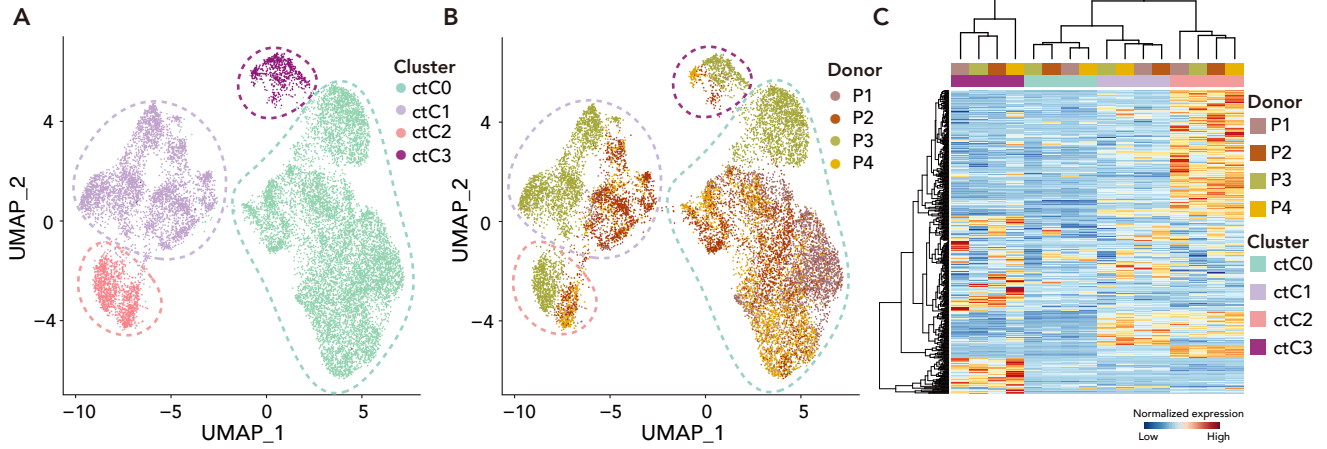
- 880 66. Aran D, Looney AP, Liu L, Wu E, Fong V, Hsu A, et al. Reference-based analysis of lung
881 single-cell sequencing reveals a transitional profibrotic macrophage. *Nature Immunology*.
882 2019;20(2):163-+.
- 883 67. Aran D, Looney AP, Liu L, Wu E, Fong V, Hsu A, et al. Reference-based analysis of lung
884 single-cell sequencing reveals a transitional profibrotic macrophage. *Nat Immunol*.
885 2019;20(2):163-72.
- 886 68. Stuart T, Butler A, Hoffman P, Hafemeister C, Papalexi E, Mauck WM, 3rd, et al.
887 Comprehensive Integration of Single-Cell Data. *Cell*. 2019;177(7):1888-902 e21.
- 888 69. Khan A, Fornes O, Stigliani A, Gheorghe M, Castro-Mondragon JA, van der Lee R, et al.
889 JASPAR 2018: update of the open-access database of transcription factor binding profiles and
890 its web framework. *Nucleic Acids Res*. 2018;46(D1):D260-D6.
- 891 70. Wilson D, Charoensawan V, Kummerfeld SK, Teichmann SA. DBD--taxonomically broad
892 transcription factor predictions: new content and functionality. *Nucleic Acids Res*.
893 2008;36(Database issue):D88-92.
- 894 71. Hu H, Miao YR, Jia LH, Yu QY, Zhang Q, Guo AY. AnimalTFDB 3.0: a comprehensive
895 resource for annotation and prediction of animal transcription factors. *Nucleic Acids Res*.
896 2019;47(D1):D33-D8.
- 897 72. Pujato M, Kieken F, Skiles AA, Tapinos N, Fiser A. Prediction of DNA binding motifs from
898 3D models of transcription factors; identifying TLX3 regulated genes. *Nucleic Acids Res*.
899 2014;42(22):13500-12.
- 900 73. Uhlen M, Fagerberg L, Hallstrom BM, Lindskog C, Oksvold P, Mardinoglu A, et al.
901 Proteomics. Tissue-based map of the human proteome. *Science*. 2015;347(6220):1260419.
- 902 74. La Manno G, Soldatov R, Zeisel A, Braun E, Hochgerner H, Petukhov V, et al. RNA velocity
903 of single cells. *Nature*. 2018;560(7719):494-8.
- 904



G 16,145 cells

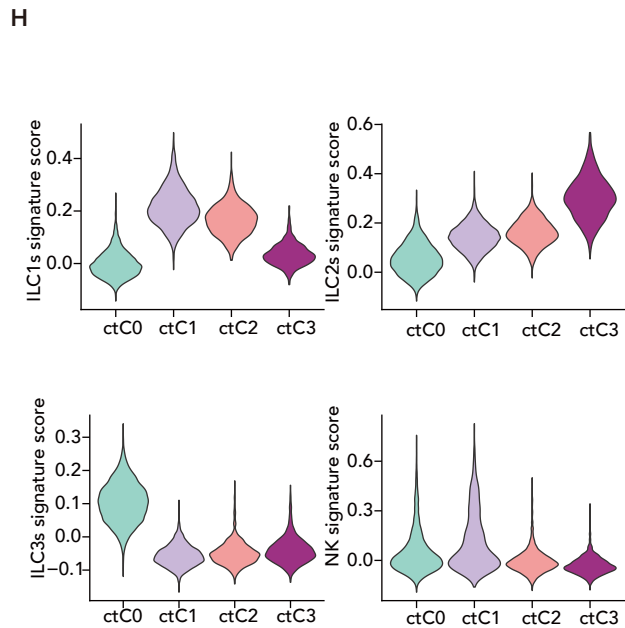
	Top 10	Transcription factors	Secreted	Cell membrane
nmC0-3	CXCL8 IL411 CD83 LST1 IL1R1 CXCL2 ATP1B3 NRP1 VEGFA NCOA7	ZFAND5 HES1 ZNF331 ATF3 RBPJ NR4A3 ID2 NFKB1 NFIL3 IRF4	CXCL8 IL411 IL1R1 CXCL2 VEGFA LGALS3 TNFRSF25 CSF2 SDC4 TNFSF13B	CD83 LST1 IL1R1 ATP1B3 PCDH9 KIT MPV17L ICOS SCN1B TNFRSF25
nmC4	GNLY KLRD1 CCL4 CMC1 NKG7 CTSW HCST EMP3 CD7 IFITM2	HOPX IRF8 CEBPB GATA3 YBX3 ZEB2	GNLY CCL4 CCL5 CTSW CST7 XCL2 LGALS1 CD55 GZMK NUCB2 TNFRSF1B	KLRD1 NKG7 HCST EMP3 CD7 IFITM2 CRTAM LITAF SELL FCER1G
nmC5	CCL4 CD3D CD3G SYNE2 CCL5 HSPA1B CD3E FYB1 TRAT1 DNAJB1	IKZF3 BCL11B BATF ZNF831 PRDM1 PBX4 ID3 SP140	CCL4 CCL5 CD40LG CST7 LGALS1 IFNG IL32 GZMM IL6ST CD6	CD3D CD3G SYNE2 CD3E TRAT1 GPR171 S100A10 CLEC2D CD48 CD40LG

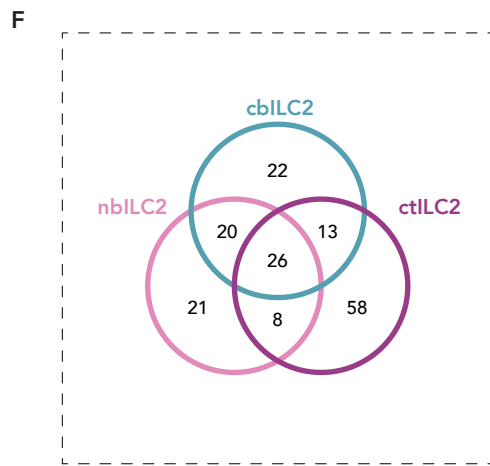
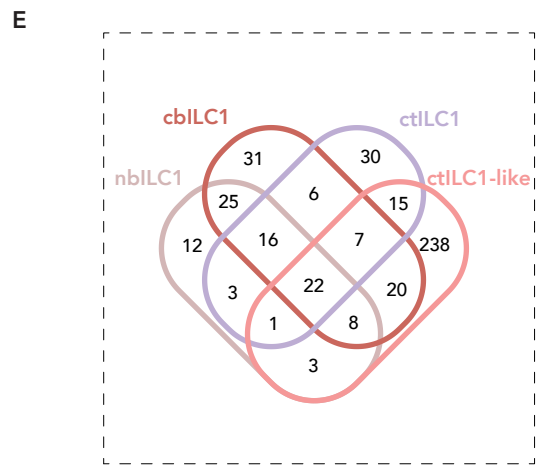
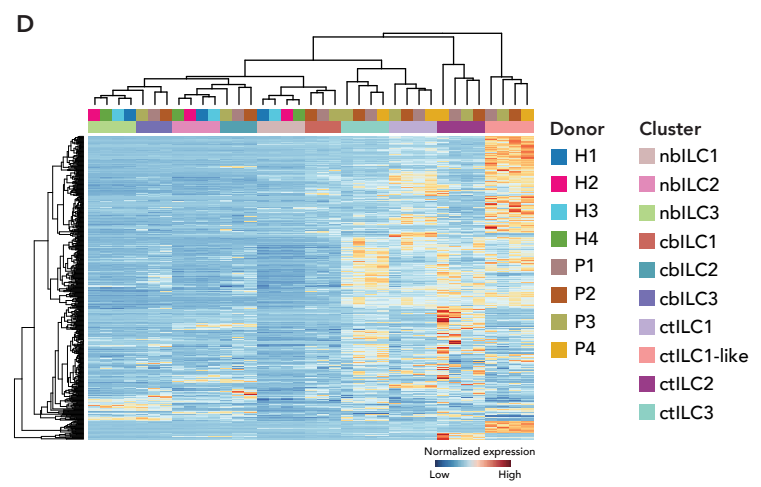
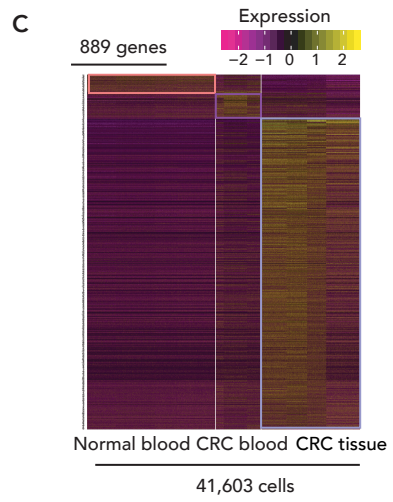
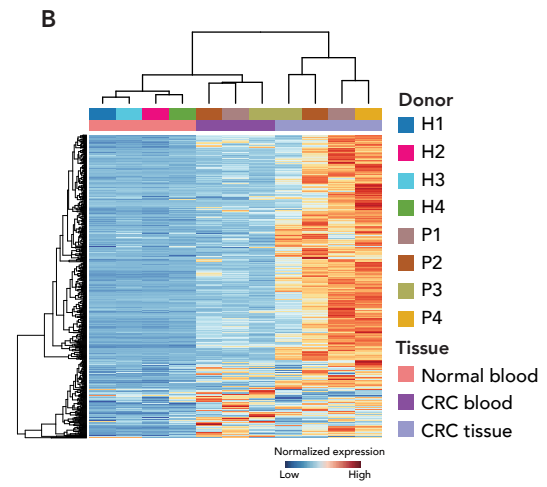
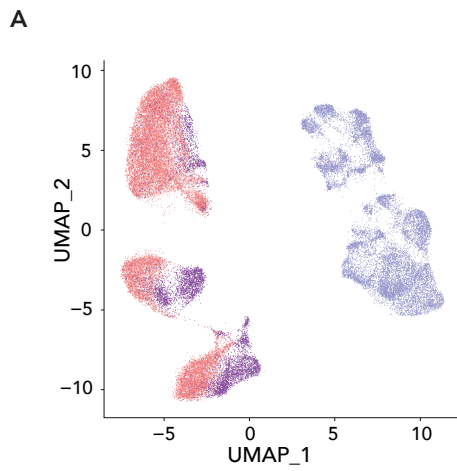


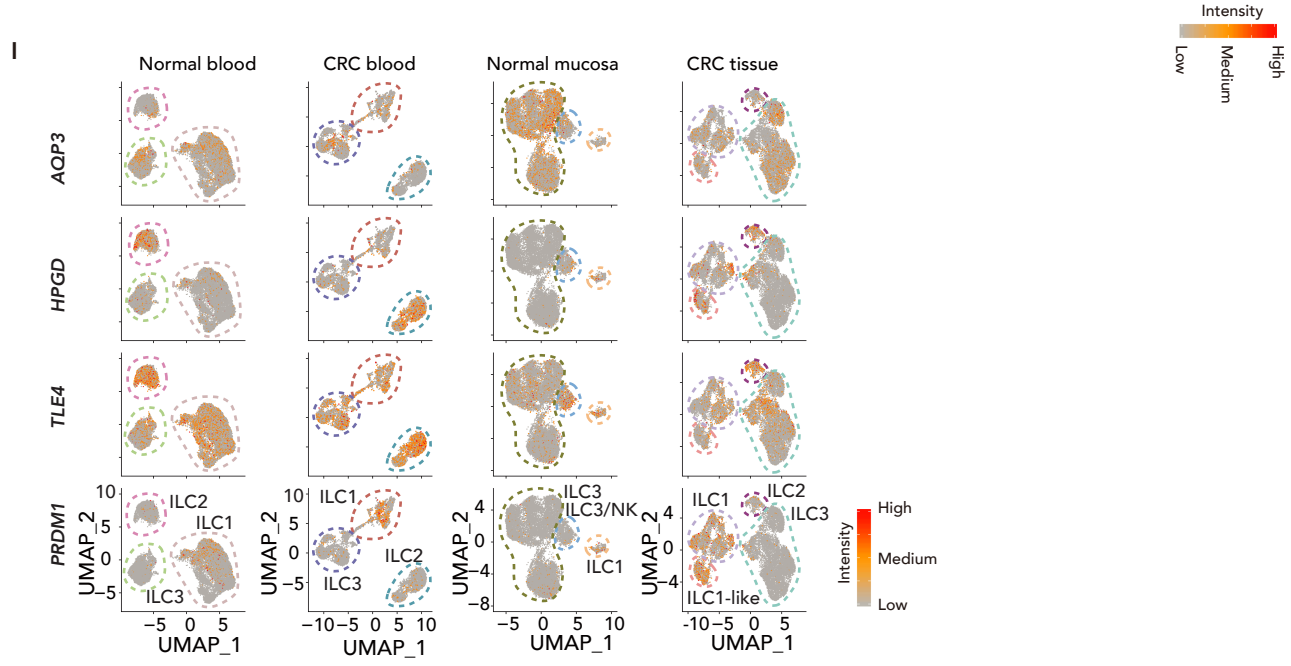
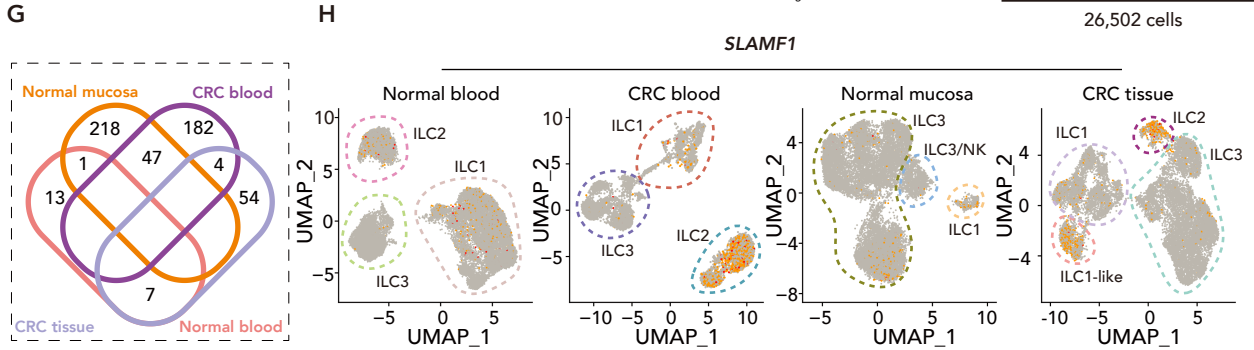
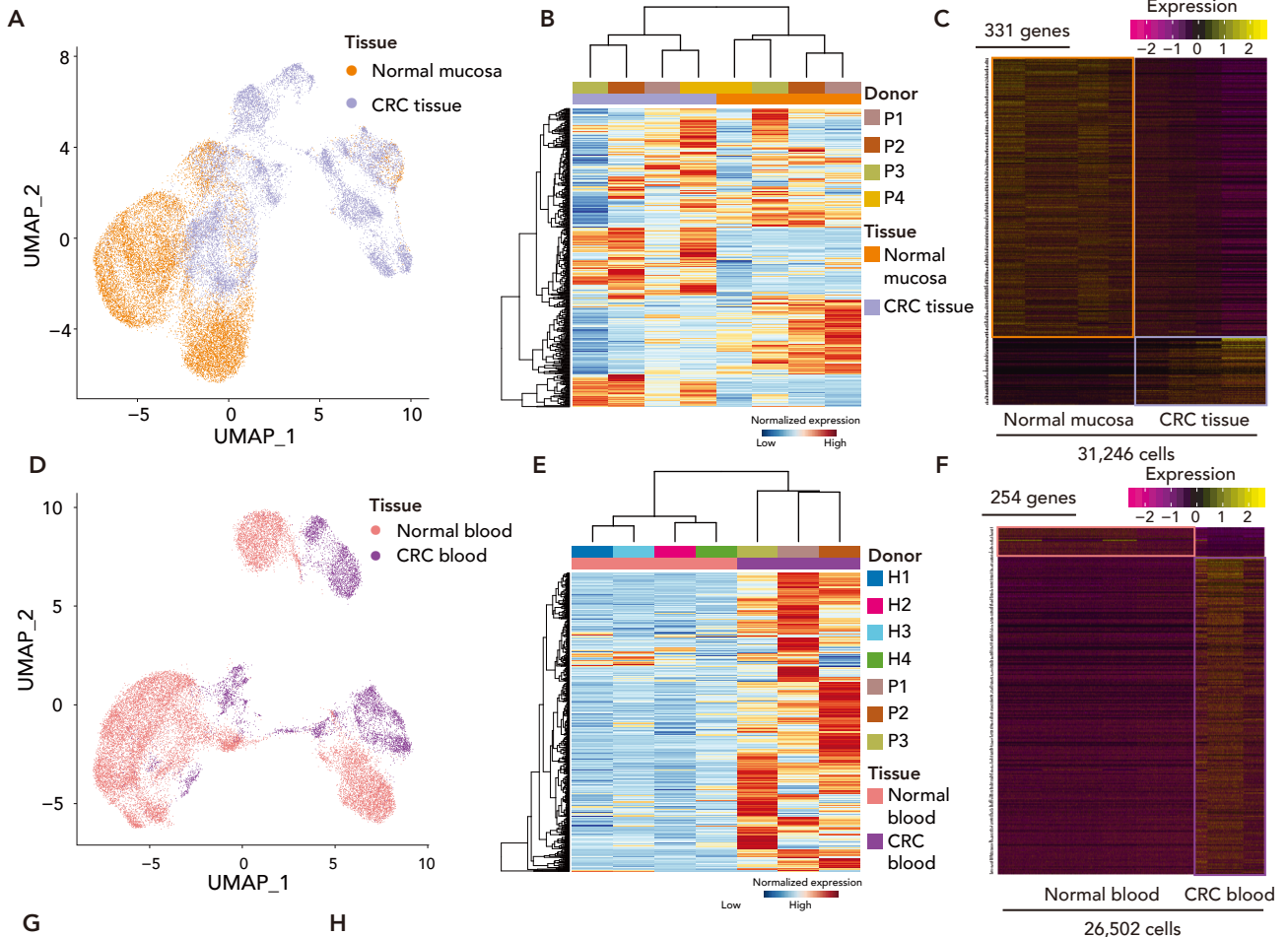


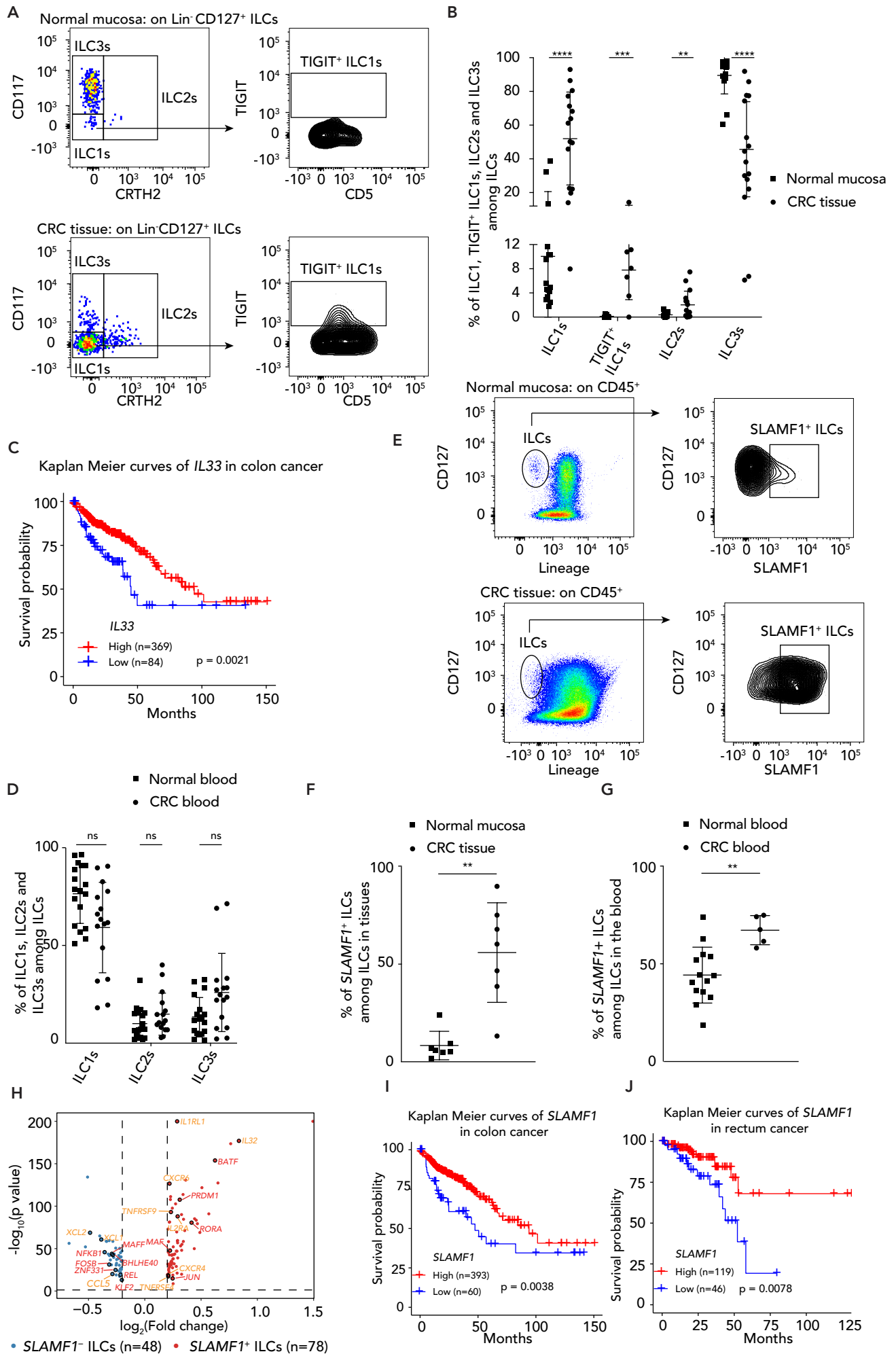
G

	Top 10	Transcription factors	Secreted	Cell membrane
ctC0	AREG KIT XCL1 GNLY XCL2 TYROBP NFKB1 CTSW CXCL8 ZFP36L1	NFKB1 MAFF FOSB REL BHLHE40 ZNF331 RBPJ NFIL3 AFF3 RERE	XCL1 GNLY XCL2 CTSW CXCL8 IL41 VEGFA EREG TNFSF11 SPINK2	AREG KIT TYROBP LST1 PCDH9 FCER1G CD81 SELENOS CD83 EREG
ctC1	CCL4 CCL4L2 GZMK CD3D IFNG CCL5 GZMA CD3G NKG7 GZMH	PRDM1 ZNF831 PBX4 BATF IKZF3 BCL11B SP140	CCL4 CCL4L2 GZMK IFNG CCL5 GZMA GZMH CST7 ANXA1 GZMM	CD3D CD3G NKG7 TRAT1 SYNE2 GPR171 CD3E RARRES3 CD40LG CD8A
ctC2	BATF TIGIT CARD16 SAT1 CTLA4 MAGEH1 CTSC LINC01943 CD27 ICA1	BATF FOXP3 PRDM1 ZBTB38 IKZF2 BLOC151 MAF CREM ETV7 PBX4	IL32 LAIR2 TNFRSF1B SLAMF1 IL1R2 LGALS1 ISG15 NAMPT C4orf48 SPOCK2	TIGIT CTLA4 MAGEH1 CD27 TNFRSF4 TNFRSF9 CLEC2D TNFRSF1B CD3D IL2RA
ctC3	IL1RL1 HPGDS SLAMF1 PLIN2 IL17RB PTGS2 PMAIP1 ZFP36L2 IL2 HPGD	GATA3 HES4 RORA ZBTB16 EGR1 PPARG KLF9	IL1RL1 SLAMF1 IL2 TNFSF10 IL32 DPP4 FSTL4 ANXA1	IL1RL1 SLAMF1 IL17RB C1orf162 CD69 KLRB1 PTGER2 CYSLTR1 FFAR3 TNFSF10

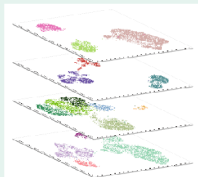






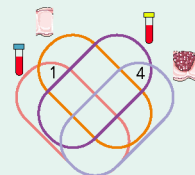
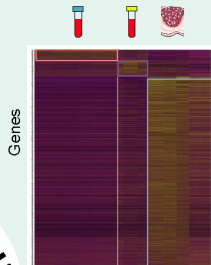


ILCs heterogeneity



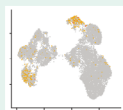
-  Normal blood
-  CRC blood
-  Normal mucosa
-  CRC tissue

Tissue-specific phenotype



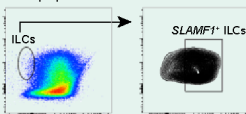
Overlapping up/down regulated genes

Gene expression



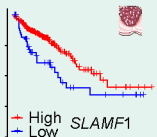
Inter-tissue common signature

Cell population



Validation & clinical relevance

Survival curve



High SLAMF1
Low